NRL Report 8792

Vertical Coherence Along a Macroray Path in an Inhomogeneous Anisotropic Ocean

J. S. PERKINS AND B. B. ADAMS

Large Aperture Acoustics Branch
Acoustics Division

and

J. J. MCCOY

The Catholic University of America
Washington, DC 20064

August 20, 1984

NAVAL RESEARCH LABORATORY
Washington, D.C.

REPORT DOCUMENTATION PAGE

1a. REPORT SECURITY CLASSIFICATION UNCLASSIFIED	1b. RESTRICTIVE MARKINGS
2a. SECURITY CLASSIFICATION AUTHORITY	3. DISTRIBUTION/AVAILABILITY OF REPORT Approved for public release; distribution unlimited.
2b. DECLASSIFICATION/DOWNGRADING SCHEDULE	
4. PERFORMING ORGANIZATION REPORT NUMBER(S) NRL Report 8792	5. MONITORING ORGANIZATION REPORT NUMBER(S)
6a. NAME OF PERFORMING ORGANIZATION Naval Research Laboratory 6b. OFFICE SYMBOL (*If applicable*) Code 5162	7a. NAME OF MONITORING ORGANIZATION
6c. ADDRESS (*City, State and ZIP Code*) Washington, DC 20375	7b. ADDRESS (*City, State and ZIP Code*)
8a. NAME OF FUNDING/SPONSORING ORGANIZATION Office of Naval Research 8b. OFFICE SYMBOL (*If applicable*)	9. PROCUREMENT INSTRUMENT IDENTIFICATION NUMBER
8c. ADDRESS (*City, State and ZIP Code*) 800 N. Quincy Street Arlington, VA 22217	10. SOURCE OF FUNDING NOS. PROGRAM ELEMENT NO.: 61153N PROJECT NO.: RR011-08-43 TASK NO.: WORK UNIT NO.: DN180-025
11. TITLE (*Include Security Classification*) (see page ii)	
12. PERSONAL AUTHOR(S) Perkins, J.S., Adams, B.B., and McCoy, J.J., (Catholic University of America)	
13a. TYPE OF REPORT Interim 13b. TIME COVERED FROM TO	14. DATE OF REPORT (*Yr., Mo., Day*) 1984 August 20 15. PAGE COUNT 40
16. SUPPLEMENTARY NOTATION	
17. COSATI CODES FIELD / GROUP / SUB. GR.	18. SUBJECT TERMS (*Continue on reverse if necessary and identify by block number*) Propagation Scattering Coherence Internal waves

19. ABSTRACT (*Continue on reverse if necessary and identify by block number*)

This report is a major output of a program in spatial properties of low-frequency acoustic fields in the deep ocean. This project was instituted at the Naval Research Laboratory in 1974 to provide a priori estimates of the capabilities and limitations of large arrays which are due to coherence degradations from environmental causes. The research has emphasized stochastic measures of irregularities in the ocean. This approach has been followed to provide probabilistic predictions of the environmental limits to aperture designs. The elements degrading the spatial coherence of an acoustic signal have been dealt with in the following order: volume effects, bottom effects, and surface effects. Specifically, this report provides the background, theoretical basis, algorithm, and operational information for a FORTRAN computer program called COVERT. This program estimates the effect of stochastic volume scattering on the vertical

(Continued)

20. DISTRIBUTION/AVAILABILITY OF ABSTRACT UNCLASSIFIED/UNLIMITED [X] SAME AS RPT [ ] DTIC USERS [ ]	21. ABSTRACT SECURITY CLASSIFICATION UNCLASSIFIED
22a. NAME OF RESPONSIBLE INDIVIDUAL John S. Perkins	22b. TELEPHONE NUMBER (*Include Area Code*) (202) 767-3173 22c. OFFICE SYMBOL Code 5162

DD FORM 1473, 83 APR EDITION OF 1 JAN 73 IS OBSOLETE

11. Title (Included Security Classification)

Vertical Coherence Along a Macroray Path in an Inhomogeneous Anisotropic Ocean

19. Abstract (Continued)

spatial coherence of an acoustic signal along a single path. The propagation path (determined by the mean sound-speed field) is part of the program input and is termed a macroray path. The scattering employed is appropriate for internal waves; i.e., it is characterized by a high degree of anisotropy, is depth dependent, and is described by a fluctuations spectrum that is characteristic of internal waves. The report summarizes the theoretical formulations on which the program is based, the numerical algorithms used, the input data required, and the outputs that are calculated. Some sample results are also included.

PREFACE

This report is a major output of a program in spatial properties of low-frequency acoustic fields in the deep ocean. This project was instituted at the Naval Research Laboratory in 1974 to provide a priori estimates of the capabilities and limitations of large arrays which are due to coherence degradations from environmental causes. The research has emphasized stochastic measures of irregularities in the ocean. This approach has been followed to provide probabilistic predictions of the environmental limits to aperture designs.

We have dealt with the contributing elements in the following order: volume effects, bottom effects, and surface effects. The latter two categories are currently under development, while the first category is dealt with in part in this report and is essentially closed at the present time. The ordering of the mechanisms and their influence has been guided by the logical separability of volume effects from those that relate to the bottom and/or the surface. The volume effects treated in this program provide the outside practical limit on resolution, and hence size, of low-frequency arrays that our present knowledge of the internal structure of the deep ocean will permit. In other words, the resolution limit caused by the forward scattering of the acoustic waves by internal inhomogeneities in the deep ocean can be estimated with the computer models developed by this program. The model provided in this report calculates the vertical coherence limitation resulting from random volume scattering. A horizontal coherence model and a more complex vertical coherence model, based on a more complete theory, have also been developed. These models are the subjects of Refs. 1 and 2.

Specifically, this report provides the background, theoretical basis, algorithm, and operational information for a FORTRAN computer program called COVERT. This program estimates the effect of stochastic volume scattering on the vertical spatial coherence of an acoustic signal along a single path. The propagation path (determined by the mean sound-speed field) is part of the program input and is termed a macroray path. The scattering employed is appropriate for internal waves; i.e., it is characterized by a high degree of anisotropy, is depth dependent, and is described by a fluctuations spectrum that is characteristic of internal waves. Our report summarizes the theoretical formulations on which the program is based, the numerical algorithms used, the input data required, and the outputs that are calculated. An historical summary of propagation in random media is contained in Appendix A.

CONTENTS

VERTICAL COHERENCE ALONG A MACRORAY PATH IN AN INHOMOGENEOUS ANISOTROPIC OCEAN

INTRODUCTION

Random environmental variations reduce the spatial coherence of an acoustic signal and thereby cause a degradation in the performance of aperture systems. This environmental loss of coherence for totally refracted paths results from stochastic volume scattering, the cause of which can be traced to temperature fluctuations. For the range of experimental parameters of interest, these fluctuations can be regarded as a direct result of internal waves. The acoustic modeling task is to relate the spatial coherence of the received signal to the three-dimensional spectrum of temperature fluctuations which is characteristic of internal waves.

As a consequence of the high degree of anisotropy of the ocean environment, the coherence length of an acoustic signal along a horizontal line transverse to the propagation direction will be much greater than along a vertical line. The coherence along a line which lies between vertical and horizontal will be between these two extremes. For frequencies below about 200 Hz, the anisotropy is such that it cannot be readily accomodated in a single coherence-loss model for a line of arbitrary tilt by simply changing a parameter. The very structure of the model will change depending on the direction of the line along which the coherence is to be estimated. The nature of the anisotropy and the presence of a background sound-speed channel greatly complicate the task of estimating signal coherence along a vertical line in comparison to the task of estimating horizontal coherence.

Considering these differences in the underlying physics, we have developed separate spatial coherence-estimating models for horizontally and vertically directed lines. FORTRAN programs based on these models have been termed COHORT [1], for a horizontally directed line, and COVERT for a vertically directed line. A third computer model [2], termed the Combined-Effects Model (CEM), also provides estimates of signal coherence for a vertically directed line. CEM propagates the mutual coherence function, with scattering, in a range-depth plane, and thus it carries forward an implicit intensity field smoothed by multiple low-angle forward scattering. Although CEM (based on a more complete theory [3]) does not have some of the limitations inherent in COVERT, it does require much more computation time.

The appropriate use of these models requires that a distinction be made between the irreversible environmental loss of coherence and the deterministic reduction of coherence along a receiving array. This deterministic reduction is caused by the combination of acoustic multipaths and nonhorizontal, nontransverse array geometry. A conventional range-stepping, parabolic-equation algorithm produces complex acoustic pressures which are then processed to model the beam power output of an array. Assuming cylindrical symmetry about the source over the sector occupied by the array, we can model arbitrary array tilts. (The array must generally be straight and transverse to the direction of propagation.) Array signal gains computed in this manner are generally less than the maximum possible, and they decrease with increasing tilt. This indicates limited coherence across the array aperture which is entirely a result of the interfering multipath field. The models discussed above conceptually and practically separate this deterministic incoherence from that generated by random volume scattering. They include vertical refraction, but *not* the effects resulting from interfering multipaths. Thus, the main purpose of these models is to predict the ultimate limits on array performance imposed by random environmental fluctuations.

Manuscript approved Nov. 4, 1983.

This report provides the background, theoretical basis, algorithm, and operational information for a FORTRAN computer program called COVERT. This program estimates the effect of stochastic volume scattering on the vertical spatial coherence of an acoustic signal along a single path. The propagation path (determined by the mean sound-speed field) is part of the program input and is termed a macroray path. The scattering employed is appropriate for internal waves; i.e., it is characterized by a high degree of anisotropy, is depth dependent, and is described by a fluctuations spectrum that approximates the Garrett-Munk spectrum [4].

The degradation in performance of line arrays due to stochastic volume scattering is most conveniently formulated in terms of the two-point coherence function $<\Gamma>$ of the complex-valued acoustic pressure field $p(z,r)$:

$$<\Gamma(z,s,r)> = <p(z + (s/2),r)p^*(z - (s/2),r)>. \tag{1}$$

Here the range coordinate is denoted by r, and the two points on the vertical line array are located by an average depth coordinate z and a separation coordinate s. The asterisk specifies complex conjugation, and the angular brackets indicate an averaging—an ensemble average in our theoretical model, a temporal average in practice. Of particular interest is the spatial Fourier transform of $<\Gamma>$:

$$<\hat{\Gamma}(z,\theta,r)> = \int_{-\infty}^{\infty} <\Gamma(z,s,r)> \exp(-ik_0\theta s)\,ds, \tag{2}$$

where k_0 is the averaged signal wave number; i.e., $k_0 = 2\pi f/c_0$, where f is the signal frequency and c_0 is an average sound speed. For an acoustic field that is statistically homogeneous across the array, $<\hat{\Gamma}>$ can be interpreted to give the directional resolution of the averaged intensity.

In the absence of a sound channel and any depth dependence of the scattering mechanism, it is possible to provide analytic expressions for $<\Gamma>$ in a number of special cases. These expressions provide useful zeroth order estimates of the loss of signal coherence because of sound-speed fluctuations caused by the presence of internal waves, provided the frequency of the acoustic signal is high enough (above several hundred Hz) [5-7] or low enough (in the range of several tens to less than a hundred Hz) [8-10]. Further, an efficient algorithm exists [3,11] which can span both the gap within which the analytic expressions cease to be valid, as well as the limiting regions for which the analytic expressions apply.

The incorporation of a sound channel and the possibility of depth-dependent statistics most certainly require the introduction of a numerical procedure. Although an appropriate theory is available [3,12,13] to provide the basis of this program and has been implemented as CEM, this implementation is very complicated, and its use requires a considerable amount of computation time. Another program which is based on a Monte Carlo integration of equations (very similar to those on which CEM is based) is also available [14]. The use of this program also requires considerable computation time. Further, this last program introduces a description of the scattering process that limits its applicability by requiring that the acoustic frequency exceed several hundred Hz.

COVERT, which is based on a simplification of the more complete theory on which CEM is based, limits the degree of coupling between the refraction resulting from an inhomogeneous background and the random volume scattering and therefore requires considerably less computation time. This reduction of computation time is bought at the cost of some loss in the expected accuracy of the predicted coherence estimates, although this loss should be smallest for the higher frequency signals for which CEM requires the greatest amounts of computation time. The two computer models are thus complementary, with COVERT providing easily obtained first estimates of array performance and CEM providing refined estimates at lower frequencies and at increased cost in computation time.

The COVERT computer model, as documented in this report, resides on a DEC VAX 11/780 computer at Code 5160, Naval Research Laboratory (NRL). There is also a version on the Texas Instruments Advanced Scientific Computer (ASC) at NRL which is available to the Navy scientific

community (for use on the ASC or transfer to another computer) through the Navy Laboratory Computer Network (NALCON).

In the next section we discuss the COVERT program, including its inputs and outputs. The final section indicates the names of the input variables and their required formats. Appendix A is an historical summary of the development of propagation in random media. Appendix B outlines the theoretical basis of COVERT and the algorithm used in its implementation at low frequencies, as determined by the value of an anisotropy ratio described in the next section. Appendix C outlines a simplification of the algorithm of Appendix B that is used in COVERT at higher frequencies. Appendix D is a reprint of Ref. 3 which contains much of the theoretical basis for COVERT. And Appendix E contains a sample set of input data and the resulting outputs.

PROGRAM DESCRIPTION

We describe the program by discussing the algorithm employed, the significance of the inputs required, and the outputs produced.

Algorithm

The program algorithm is based on an intuitive argument that the principal effects of the inhomogeneous sound-speed profile on the loss of spatial coherence because of stochastic volume scatter are limited to two factors. One is a change in the orientation of the macroray segments relative to the highly anisotropic scattering mechanism, and the second is a shift in the vertical position of the segments relative to the depth-dependent scattering strength. The former factor affects both the rate at which scattering occurs and the degree to which the scattered signal loses coherence; the latter factor affects only the rate at which the scattering occurs, i.e., the range required for volume scatter to be significant. Flatté et al. [7] suggested that the results obtained in the absence of a sound channel and with depth-independent statistics could be extended by simply replacing the line from source to receiver by a curved macroray path. Beran et al. [13] discussed the validity of that suggestion within the context of a more complete radiative transport theory. COVERT, then, is based on a suggestion by Flatté et al. and further replaces the curved macroray path by a sequence of straight segments. The evolution of $<\hat{\Gamma}(z,\theta,r)>$ over a single segment is calculated as if there were no sound channel and as if the statistics were homogeneous.

The numerical algorithm for propagating $<\hat{\Gamma}(z,\theta,r)>$ over a single segment depends on the frequency of the signal and on the description of the environment. Accordingly, we define a nondimensional anisotropy ratio $\alpha = k_0 l_V^2 / l_H$ where l_V and l_H are characteristic dimensions of the sound-speed fluctuations as measured along vertical and horizontal lines. For small values of this ratio, i.e., at low frequencies, the high anisotropy of the scattering mechanism is of fundamental significance, and this leads to a complicated numerical algorithm that solves an integrodifferential equation by iteration. Although we refer to this procedure as the low-frequency algorithm, the limitation is practical rather than theoretical. We present the theoretical basis for this algorithm in Appendix B. At high enough frequencies, which correspond to large values of α, the anisotropy of the scattering mechanism is not of fundamental significance, and a much simpler numerical algorithm, which is algebraic in character, can be used. The approximation on which this simpler algorithm is based is discussed in Appendix D, which is a reprint of Ref. 3, and the formulation is summarized in Appendix C.

The value of α where the program switches from the low-frequency algorithm to the high-frequency algorithm has been set at 2.0. The results of the high-frequency algorithm are sufficiently accurate for $\alpha \geqslant 2.0$; they agree with the results of the low-frequency algorithm when $\alpha = 2.0$ (see Appendix E). For $\alpha > 2.0$, the numerical integration of the low-frequency algorithm may require a finer grid than the default established in the program. Also, the time for convergence of the iteration

procedure increases rapidly with frequency. For $\alpha < 2.0$, the approximation included in the high-frequency algorithm is less accurate. The low-frequency algorithm is reasonably fast for these lower frequencies.

COVERT calculates $<\hat{\Gamma}(z,\theta,r)>$ only at the endpoints of the segments of the macroray path; i.e., COVERT calculates $<\hat{\Gamma}(z_r,\theta,r)>$ as a function of θ, where z_r is the depth of the macroray path at range r. The values of $<\hat{\Gamma}>$ calculated for the end of one segment are used as the input for the next segment. The values of $<\hat{\Gamma}(z_r,\theta,r)>$ must be shifted along the θ axis at the transition from one segment to the next so that the peak is at the angle corresponding to the direction of propagation. This models a (discontinuous) change in the direction of the signal as it follows the piecewise-linear approximation of the macroray path.

Although the strength of the scattering mechanism is assumed constant over each segment (and equal to the value at the midpoint of the segment) it is allowed to vary with the depth of the segment. The vertical and horizontal correlation lengths, l_V and l_H (which are required inputs), could be allowed to vary with depth in a similar manner, but this has not been implemented. Following Desaubies [15], we estimate that typical values for these lengths at depths near 100 m are 3600 m horizontally and 95 m vertically. McCoy and Beran [3] used 7000 m and 100 m in investigating the effects of anisotropy, and these values are used in the sample runs in Appendix E.

To numerically model the source consistent with a plane wave traveling in the direction of the first segment of the macroray path, COVERT assumes that

$$<\hat{\Gamma}(z_0,\theta,0)> = I/(\sqrt{\pi}\,\theta_c)\,\exp\,[-(\theta-\theta_i)^2/\theta_c^2], \tag{3}$$

where θ_i is the angle that the first segment makes with the horizontal and θ_c is a characteristic angular source width which is set at 0.01° by the program. The description of the source is discussed further in Appendixes B and C.

Input Data Required

A macroray path from the source to the receiver along which COVERT is to propagate $<\hat{\Gamma}>$ is input by specifying the endpoints of the sequence of path segments. Such a segmented ray path can be obtained from a ray-trace program such as TRIMAIN [16]. For a multipath structure, the individual macroray paths must be treated separately.

The source frequency and two lengths (l_V and l_H) that characterize correlation distances for the refractive-index-fluctuations field in the horizontal and vertical directions must be specified.

The strength of the refractive-index fluctuations is described by a nondimensional environmental parameter ϵ^2. Appendix B defines this parameter and shows how it is related to the environmental parameter E used by the COHORT program [1]. Although COHORT uses a depth-averaged value of E, the COHORT program can be used to estimate E as a function of depth from whatever environmental data may be available (such as a temperature profile). A table (profile) that describes $E(z)$ is required by COVERT, and the program makes the conversion to ϵ^2. E has a typical value of 10^{-10}.

A complete listing of the input data and the required formats are given in the section entitled **INPUT VARIABLES AND FORMATS**.

Outputs Calculated

Two measures of the received signal are calculated and plotted. The *Totai Signal* is the distribution of $<\hat{\Gamma}(z_R,\theta,R)>$ as a function of θ where (z_R,R) is the receiver point (the last point on the

macroray path). The *Normalized Scattered Signal* $<\hat{\Gamma}>_N$ is the *Total Signal* minus a scaled replica of the initial signal, normalized so that the maximum value is 1.0. The intent is to subtract from the received signal that portion that can be considered to have undergone no scattering. The scaling for the replica of the initial signal is determined by the normalized range of the problem which depends on the strength of the scattering and on the lengths and angles (with respect to horizontal) of the segments of the macroray path. A normalized range of 1.0 is defined by the condition that the intensity of the coherent portion of the signal has been reduced by a factor of $1/e$. If the high-frequency (quasi-isotropic) calculation is used, then $<\Gamma(z_R,s,R)>$ is also plotted (as a function of s).

A measure of the coherence of the received signal is given by the curvature of the normalized scattered signal $<\hat{\Gamma}(z_R,\theta,R)>_N$ at the main arrival angle θ_A. We define the coherence length by

$$L = \frac{1}{k_0}\left|\frac{1}{<\hat{\Gamma}>_N}\,\frac{d^2<\hat{\Gamma}>_N}{d\theta^2}\right|^{1/2}_{\theta=\theta_A}. \tag{4}$$

This length is part of the program output and is termed the final characteristic length. The angular width of $<\hat{\Gamma}(z_R,\theta,R)>$ is also output.

INPUT VARIABLES AND FORMATS

The input variables with brief descriptions are listed below. The required input sequence follows this list.

FREQ — The source frequency (Hz)

XLH — The horizontal correlation length (m) of the refractive-index field

XLV — The vertical correlation length (m) of the refractive-index field

NEPTS — The number of points on the profile describing the strength of the refractive-index fluctuations as a function of depth. ($2 \leqslant$ NEPTS $\leqslant 51$.)

EDEP(I) — The Ith depth on the refractive-index fluctuations profile. ($I = 1, 2, \ldots,$ NEPTS.)

EVAL(I) — The strength of the refractive-index fluctuations at depth EDEP(I). ($I = 1, 2, \ldots,$ NEPTS.)

NSEG1 — The number of points describing the macroray path. NSEG1 is equal to the number of segments on the macroray path plus one. ($2 \leqslant$ NSEG1 $\leqslant 3001$.)

RANGE(I) — The range (km) of the Ith point on the segmented macroray path. Thus, RANGE(1) should be 0.0 and RANGE(NSEG1) is the range of the receiver. ($I = 1, 2, \ldots,$ NSEG1.)

DEPTH(I) — The depth (m) of the macroray path at RANGE(I). ($I = 1, 2, \ldots,$ NSEG1.)

These variables are integers or floating-point numbers according to the usual FORTRAN convention and are input as card images in the following order with free format:

FREQ, XLH, XLV
NEPTS
EDEP(I), EVAL(I), I = 1, NEPTS (may require several cards)
NSEG1
RANGE(I), DEPTH(I), I = 1, NSEG1 (may require several cards)

REFERENCES

1. L.B. Palmer, D.M. Dundore, B.B. Adams, and J.J. McCoy, "Transverse Horizontal Coherence and Low-Frequency Array Gain Limits in the Deep Ocean," NRL Report 8695, Aug. 1983.

2. R.N. Baer, J.S. Perkins, E.B. Wright, and J.J. McCoy, "Stochastic Propagation of the Mutual Coherence Function in the Deep Ocean," *J. Acoust. Soc. Am.* **75**, 1407-1414 (1984).

3. J.J. McCoy and M.J. Beran, "Directional Spectral Spreading in Randomly Inhomogeneous Media," *J. Acoust. Soc. Am.* **66**, 1468-1481 (1979).

4. C. Garrett and W.H. Munk, "Space-Time Scales of Internal Waves: A Progress Report," *J. Geophys. Res.* **80**, 291-297 (1975).

5. M.J. Beran, "Propagation of the Mutual Coherence Function Through Random Media," *J. Opt. Soc. Am.* **56**, 1475-1480 (1966).

6. V.I. Tatarskii, "The Effects of the Turbulent Atmosphere on Wave Propagation," translated from the Russian and available from National Technical Information Service, Springfield, Va., TI-68-5064 (1971).

7. S.M. Flatté, R. Dashen, W.H. Munk, K.M. Watson, and F. Zachariasen, *Sound Transmission Through a Fluctuating Ocean* (Cambridge University Press, Cambridge, 1979).

8. M.J. Beran and J.J. McCoy, "Propagation Through an Anisotropic Random Medium," *J. Math. Phys.* **15**, 1901-1912 (1974).

9. M.J. Beran and J.J. McCoy, "Propagation Through an Anisotropic Random Medium. An Integro-Differential Formulation," *J. Math. Phys.* **17**, 1186-1189 (1976).

10. M.J. Beran, J.J. McCoy, and B.B. Adams, "Effects of a Fluctuating Temperature Field on the Spatial Coherence of Acoustic Signals," NRL Report 7809, May 1975.

11. N. Schwartz and M. J. Beran, "Scattering in an Anisotropic Random Medium: Numerical Calculation," *J. Acoust. Soc. Am.* **65**, 1386-1391 (1979).

12. I.M. Besieris and F.D. Tappert, "Stochastic Wave-Kinetic Theory in the Liouville Approximation," *J. Math. Phys.* **17**, 734-743 (1976).

13. M.J. Beran, A.M. Whitman, and S. Frankenthal, "Scattering Calculations Using the Characteristic Rays of the Coherence Function," *J. Acoust. Soc. Am.* **71**, 1124-1130 (1982).

14. H.L. Wilson and F.D. Tappert, "Acoustic Propagation in Random Oceans Using the Transport Equation," Science Applications, Inc., Report SAI-78-639-LJ, La Jolla, Calif. (Apr. 1978).

15. Y.J.F. Desaubies, "On the Scattering of Sound by Internal Waves in the Ocean," *J. Acoust. Soc. Am.* **64**, 1460-1469 (1978).

16. B.G. Roberts Jr., "Horizontal-Gradient Acoustical Ray-Trace Program TRIMAIN," NRL Report 7827, Dec. 1974.

Appendix A

HISTORICAL SUMMARY OF PROPAGATION IN RANDOM MEDIA

1940s AND 1950s

The modern history of research on the scattering of a radiation field by a randomly fluctuating continuum began during and immediately after World War II. A number of significant studies reported then by Bergmann [A1], Mintzer [A2], and Pekeris [A3] were undertaken to explain observations of the effects of temperature fluctuations in the ocean on a propagating acoustic signal. Since these fluctuations were weak, and the range of the experiments of interest was limited, the principal method of analysis was a single-scatter theory, or a Born approximation. Subsequent to these experiments, a number of conceptually and mathematically similar studies were motivated by observations of the effects of atmospheric turbulence on a propagating laser-beam signal.

Two monographs, by Chernov [A4] and by Tatarskii [A5], were translated into English and published in 1960 and 1961. These books provided a rather complete survey of the research that had been carried out in the Soviet Union, and they defined the state of the art at that time. The research discussed pertained to both acoustic and electromagnetic radiation and emphasized the importance of turbulence as the dynamic process that ultimately gives rise to the scattering. The manuscript by Tatarskii was particularly noteworthy for its description of the fluctuating medium and for its reliance on the Kolmogorov spectrum as a correct description of the scattering mechanism. Both monographs were also significant for introducing the Rytov approximation of random-scattering problems to Western researchers. The Rytov approximation, like the Born approximation, is based on perturbation ideas, but the claim of both authors was that the approximation correctly accounted for the multiple scattering effects necessary for the calculations to be valid for long ranges.

1960s

Research into the subject went through a high point in activity and in controversy during the 1960's with most of the reported studies treating the scattering of electromagnetic signals in the atmosphere. Much of the controversy centered around two questions: What measures of the statistics of the radiation field are most conveniently determined in physical experiments and most conveniently incorporated in theories? How does one derive theories that properly incorporate multiple scatter effects, as well as the effects of diffraction? A number of studies of the second question were framed in terms of the relative merits of the Born and Rytov approximations.

By the close of the decade of the 1960's the controversy on these fundamental questions largely ceased. The central role of the multipoint statistical moments, termed coherence functions in the propagation literature, was recognized by increasing numbers of researchers. Techniques were developed for deriving theories, in the form of partial differential equations, governing these statistical moments. Specific equations were written for the second- and fourth-order moments, the most crucial moments for discussing experiments. And studies were frequently reported treating the analysis and the solution of these equations in specific applications. A second monograph by Tatarskii [A6], which appeared in English in 1971, deemphasized the role of the Rytov approximation highlighted in the earlier work. The position espoused in this second monograph appeared to be quite similar to that reached by a growing number of researchers in the United States.

1970s

Extensions of the Theory—Research in the 1970s addressed the need to solve the governing field equations on the second- and fourth-order moments. These efforts included obtaining analytic solutions for idealized experiments and developing the general numerical algorithms needed to address realistic experiments. Also, special attention was again given to the scattering of acoustic signals in the ocean. While, in principle, scattering of ocean acoustic signals and scattering of atmospheric electromagnetic signals are the same, four factors distinguish specific ocean acoustic experiments from specific atmospheric electromagnetic experiments. First, the specific statistic to be estimated for the ocean acoustic experiment frequently differs from that of interest in the electromagnetic experiments. Second, the dynamic process that gives rise to the fluctuating continuum is different in the ocean acoustic application [A7]. Third, the wavelengths of the acoustic signals for the experiments of interest are large (relative to important characteristic lengths) compared to previous applications. And fourth, the ocean is an inhomogeneous and a highly anisotropic propagation medium [A8,A9,A10]. While the second and third of these factors make the ocean acoustic experiment different from the previous application in degree, the first and fourth can make it different in kind. It is clear that a change in the specific statistic that is of interest would change the nature of the prediction model. But it is even less clear (although equally true) that the incorporation of inhomogeneity and anisotropy of the medium introduces additional length scales that need to be parameterized in additional nondimensional ratios. Valid prediction modeling usually requires different models for different limiting values of these nondimensional ratios.

As we continue with a synopsis of the advances made in the 1970s, we find that researchers achieved a general appreciation of the mathematical identity of the scattering of acoustic signals in the ocean by a randomly inhomogeneous continuum and the quantized motion of a particle in a randomly perturbed potential field [A11,A12], as well as a duality between a radiative transport theory and the equation governing the two-point coherence function [A13-A15]. While this appreciation has not greatly altered the general flow of the development of theories, it has introduced new techniques that could prove useful in solving specific problems, e.g., the use of Monte Carlo calculations [A16]. Two additional analytic techniques were introduced into the literature of stochastic volume scattering in the 1970s. One was the use of the formalism of Feynman path integrals [A17]. As applied to calculations of statistical moments of the acoustic field, path integrals provide an alternate representation of the field equations discussed above. The advantages of this representation are the natural geometric interpretation of the processes of refraction and scattering and the global nature of the approximations used to obtain numerical algorithms. The other technique was the formulation of the scattering problem in terms of a modal expansion; the scattering mechanism, in this formulation, results in a coupling via intermodal energy transfer of the normal modes defined for a depth-dependent background medium [A18-A21]. The motivation for the modal expansion formulation was, clearly, a realization that the ocean environment does define a waveguide, which becomes more obvious with the decreasing frequencies dictated by changing applications.

Specific Extended-Study Programs—A number of extended-study programs of the random scattering of acoustic signals by temperature fluctuations were carried out throughout the 1970s. Perhaps the most exhaustive, and certainly the most extensively reported, were the studies of the JASON group; a readable summary of much of their effort has been published in book form [A22]. (An updated summary article is also available [A23].) The JASON studies made four significant contributions.

- Emphasis was placed on the need to relate the acoustic event (the stochastic scattering) to the oceanographic events (a depth-dependent background sound-speed profile and the presence of internal waves as the controlling dynamic process).

- Researchers recognized the need to combine important characteristic length scales into nondimensional parameters which could then be used to classify scattering experiments according to separate domains of parameter space. Since the JASON-group research

accepts the validity of a model that is rigorously derived for a medium that is both homogeneous and isotropic, only two nondimensional parameters are required to classify all scattering experiments: one is the ratio of the experimental range to that at which diffraction effects become significant, and the other is the ratio of the experimental range to that at which significant acoustic energy (one-half of the original energy) has been scattered.

- The Feyman path formalism already alluded to above was introduced.

- A number of reported experiments were discussed in detail, principally those of Ellinthorpe et al. [A24] and Ewart [A25].

Although the basic formalism presented by the JASON group can be applied to a broad spectrum of experiments, it has been applied in detail only to experiments in which the spatial resolution of the signal was not a principal objective. Almost all of the comparisons considered the statistics of a time series measured at a single point in the acoustic field.

A second extended program of studies was carried out by a less well-defined group, centered primarily either at New York University or around Tappert (for example, see Refs. A11-13,A16,A20,A21). The scope of the program carried out by Tappert et al. was more limited than that of the JASON group; Tappert was essentially interested in the lower order spatial statistics, or in the aperture problem that motivated much of the electromagnetic work of the 1950s and 1960s. Further, this second effort was exclusively either analytical or numerical in nature; no reference was made to any specific series of experiments. The principal contributions were noted earlier in this synopsis: namely, elucidation of the relationship between the ocean acoustics problem and that of the quantized motion of a particle in a perturbed potential field [A11,A12], the use of Monte Carlo calculations [A16], and the formulation of the scattering problem in terms of a modal expansion [A20,A21].

The third program of studies was carried out by researchers at NRL and by Beran and McCoy working with NRL. Once again the scope of the study program was limited to estimation of the spatial coherence across a receiving aperture. A series of sea tests provided the core for the program of studies, and the model development was accomplished with these sea tests in mind. Four contributions resulted from this study.

- Researchers demonstrated that the degree of anisotropy of the scattering mechanism, i.e., that caused by internal waves, was sufficient to introduce a new nondimensional ratio (which we discuss in the section entitled **Algorithm**) to completely parameterize ocean acoustic experiments [A8-A10]. The scattering models presented in the optical literature of the 1960s, or by the JASON group in the 1970s, are valid for large values of this anisotropy ratio. This limit is justified either for propagation in an isotropic medium or for the propagation of high-frequency signals. (For typical experiments, high frequency implies greater than a few hundred Hz.)

- The NRL group made a number of approximations to develop a closed-form expression for estimating the loss of spatial coherence along a transverse horizontal line array [A8,A10,A26]. Also two computer models with different levels of complexity were developed to estimate coherence along a vertical line array. One of these models is the subject of this report, while the other is the subject of Ref. 2.

- All available archival data on the loss of spatial coherence along a horizontal line array were compiled, and comparisons were made to predictions of the closed-form solution discussed above.

- A number of sea tests intended to answer specific questions raised by projected naval applications were carried out. These tests provided further justification of the closed-form solution and demonstrated its usefulness in analyzing the performance of operational or proposed aperture systems.

The volume scattering work of NRL, Beran, and McCoy has been assembled and will be published in book form [A27].

REFERENCES

A1. P.G. Bergmann, "Propagation of Radiation into a Medium with Random Inhomogeneities," *Phys. Rev.* **70**, 486-492 (1946).

A2. D. Mintzer, "Wave Propagation in a Randomly Inhomogeneous Medium. I," *J. Acoust. Soc. Am.* **25**, 922-927 (1953).

A3. C.L. Pekeris, "Note on the Scattering of Radiation in an Inhomogeneous Medium," *Phys. Rev.* **71**, 268-269 (1942).

A4. L.A. Chernov, "Wave Propagation in a Random Medium," translated by R.A. Silverman (McGraw-Hill, N.Y., 1960).

A5. V.I. Tatarskii, "Wave Propagation in a Turbulent Medium," translated by R.A. Silverman (McGraw-Hill, N.Y., 1961).

A6. V.I. Tatarskii, "The Effects of the Turbulent Atmosphere on Wave Propagation," translated from the Russian and available from National Technical Information Service, Springfield, Va., TI-68-5064 (1971).

A7. W. Munk and F. Zachariasen, "Sound Propagation Through a Fluctuating Ocean: Theory and Observation," *J. Acoust. Soc. Am.* **59**, 818-838 (1976).

A8. M.J. Beran and J.J. McCoy, "Propagation Through an Anisotropic Random Medium," *J. Math. Phys.* **15**, 1901-1912 (1974).

A9. M.J. Beran and J.J. McCoy, "Propagation Through an Anisotropic Random Medium. An Integro-Differential Formulation," *J. Math. Phys.* **17**, 1186-1189 (1976).

A10. M.J. Beran and J.J. McCoy, "Propagation of Radiation From a Finite Beam or Source Through an Anisotropic Random Medium," *J. Acoust. Soc. Am.* **56**, 1667-1672 (1974).

A11. I.M. Besieris and F.D. Tappert, "Stochastic Wave-Kinetic Theory in the Liouville Approximation," *J. Math. Phys.* **17**, 734-743 (1976).

A12. I.M. Besieris and F. Tappert, "Kinetic Equations for the Quantized Motion of a Particle in a Randomly Perturbed Potential Field," *J. Math. Phys.* **14**, 1829-1836 (1973).

A13. F.D. Tappert, "Diffractive Ray Tracing of Laser Beams," *J. Opt. Soc. Am.* **66**, 1368-1373 (1976).

A14. J.J. McCoy and M.J. Beran, "Propagation of Beamed Signals Through Inhomogeneous Media: A Diffraction Theory," *J. Acoust. Soc. Am.* **59**, 1142-1149 (1976).

A15. J.J. McCoy and M.J. Beran, "Directional Spectral Spreading in Randomly Inhomogeneous Media," *J. Acoust. Soc. Am.* **66**, 1468-1481 (1979).

A16. H.L. Wilson and F.D. Tappert, "Acoustic Propagation in Random Oceans Using the Transport Equation," Science Applications, Inc., Report SAI-78-639-LJ, La Jolla, Calif. (Apr. 1978).

A17. R. Dashen, "Path Integrals for Waves in Random Media," *J. Math. Phys.* **20**, 894-920 (1979).

A18. G.R. Sutton and J.J. McCoy, "Scattering of Acoustic Signals by Inhomogeneities in a Waveguide—A Single Scatter Treatment," *J. Acoust. Soc. Am.* **60**, 833-839 (1976).

A19. G.R. Sutton and J.J. McCoy, "Spatial Coherence of Acoustic Signals in Randomly Inhomogeneous Waveguides—A Multiple-Scatterer Theory," *J. Math. Phys.* **18**, 1052-1057 (1977).

A20. L.B. Dozier and F.D. Tappert, "Statistics of Normal Mode Amplitudes in a Random Ocean. I. Theory," *J. Acoust. Soc. Am.* **63**, 353-365 (1978).

A21. L.B. Dozier and F.D. Tappert, "Statistics of Normal Mode Amplitudes in a Random Ocean. II Computations," *J. Acoust. Soc. Am.* **64**, 533-547 (1978).

A22. S.M. Flatté, R. Dashen, W.H. Munk, K.M. Watson, and F. Zachariasen, *Sound Transmission Through a Fluctuating Ocean* (Cambridge University Press, Cambridge, 1979).

A23. S.M. Flatté, "Wave Propagation Throughout Random Media: Contributions from Ocean Acoustics," Proc. IEEE, **71**, 1984, pp. 1267-1294.

A24. A.W. Ellinthorpe et al., Naval Underwater Systems Center Technical Memoranda associated with the Joint Oceanographic Acoustic Experiment, 1975-1977.

A25. T.E. Ewart, "Acoustic Fluctuations in the Open Ocean—A Measurement Using a Fixed Refracted Path," *J. Acoust. Soc. Am.* **60**, 46-59 (1976).

A26. L.B. Palmer, D.M. Dundore, B.B. Adams, and J.J. McCoy, "Transverse Horizontal Coherence and Low-Frequency Array Gain Limits in the Deep Ocean," NRL Report 8695, Aug. 1983.

A27. R.N. Baer, B.B. Adams, M.J. Beran, D.H. Berman, K.M. Guthrie, J.J. McCoy, and J.S. Perkins, *Performance of Sonar Antennas in the Presence of Ocean Volume Scatter*, Accepted for Publication, Springer-Verlag.

Appendix B
NUMERICAL ALGORITHM

The theoretical basis for COVERT is outlined in Ref. 3, which is reprinted in Appendix D. Detailed derivations of the forumlation that forms this basis are presented in the references contained in that reprint. As discussed in this report the propagation/scattering model (designed for use when $\alpha < 2.0$) is formulated in terms of $<\hat{\Gamma}(z,\theta,r)>$, which, in the absence of an inhomogeneous background profile, satisfies

$$\frac{\partial <\hat{\Gamma}>}{\partial r} + \frac{\theta \partial <\hat{\Gamma}>}{\partial z} = \frac{-k_0}{8\pi} \left[\bar{\sigma}_V(\theta) <\hat{\Gamma}(z,\theta,r)> - \int \tilde{\sigma}_V(\theta,\theta') <\hat{\Gamma}(z,\theta',r)> d\theta'\right] \tag{B1}$$

where

$$\tilde{\sigma}_V(\theta,\theta') = k_0^2 \int \sigma(u_H,u_V) \exp\left\{ik_0\left[(\theta-\theta')u_V - \frac{1}{2}(\theta^2 - \theta'^2)u_H\right]\right\} du_H du_V \tag{B2}$$

and

$$\bar{\sigma}_V(\theta) = \int \tilde{\sigma}_V(\theta,\theta') d\theta'. \tag{B3}$$

The function $\sigma(u_H,u_V)$ describes the correlation function of the randomly varying component of the wave number, $k(r,z)$. That is

$$k^2(r,z) = k_0^2 [1 + \mu(r,z) + \Delta\mu(r,z)], \tag{B4}$$

and

$$\sigma(u_H,u_V) = <\Delta\mu(r + u_H, z + u_V)\Delta\mu(r,z)>, \tag{B5}$$

where μ denotes the deterministic or background component of the wave number field and $\Delta\mu$ denotes the randomly varying component. For a $k(r,z)$ that results from the presence of an internal wave field in the deep ocean, an appropriate choice for σ is

$$\sigma(u_H,u_V) = \epsilon^2 \exp(-|u_V|/l_V - |u_H|/l_H), \tag{B6}$$

where l_V an l_H are characteristic dimensions of the sound-speed fluctuations as measured along vertical and horizontal lines, and ϵ^2 provides a measure of the strength. Note that

$$\epsilon^2 = \sigma(0,0) = <\Delta\mu^2> = 4<(\Delta c/c)^2> \approx 4<\left[\frac{1}{c}\frac{\partial c}{\partial T}\right]^2> <\Delta T^2>, \tag{B7}$$

where c is the speed of sound and T is temperature.

ϵ^2 can be related to the environmental parameter of COHORT [B1] as follows. Using Eqs. (31) and (32) of Ref. B2 with σ as in Eq. (B6), it follows that $\epsilon^2 = \pi A^2 l_H$. The parameter E for a plane-wave source is defined in Ref. B3 as $E_{PW} = 1.1A^2 l_V$. (Also see Eq. (38) of Ref. B2.) Thus, $\epsilon^2 = \pi(l_H/l_V)E_{PW}/(1.1)$. The E parameter in COHORT, which we denote by E_{PT}, is defined however for a point source and $E_{PW} = 2.5\,E_{PT}$. (See Eqs. (39) and (40) in Ref. B2.) Now, $\epsilon^2 = \pi(l_H/l_V)(2.5/1.1)E_{PT}$. Using $A_T^2 = A^2 <\Delta T^2>/<\Delta\mu^2>$ and Eq. (B7),

$$\begin{aligned} E_{PT} &= 0.44\, A^2 l_V \\ &= 0.44\, A_T^2 l_V <\Delta\mu^2>/<\Delta T^2> \\ &= 0.44\, A_T^2 l_V 4 <(\Delta c/c)^2>/<\Delta T^2> \\ &= 1.76\, A_T^2 l_V <\left[\frac{1}{c}\frac{\partial c}{\partial T}\right]^2>, \end{aligned} \tag{B8}$$

which is the formula presented in Ref. B1 and used by the COHORT program. COVERT converts the input E_{PT} values to ϵ^2.

An ideal plane-wave source is described by the initial condition

$$<\hat{\Gamma}(z,\theta,0)> = I\delta(\theta - \theta_i) \tag{B9}$$

where I is a measure of the source strength, and θ_i directs the source. A more realistic initial condition, and one required by a numerical solution of Eq. (B1), is given by

$$<\hat{\Gamma}(z,\theta,0)> = I/(\sqrt{\pi}\,\theta_c)\ \exp\,[-\,(\theta - \theta_i)^2/\theta_c^2], \tag{B10}$$

where θ_c is a characteristic angular source width. For either initial condition, $<\hat{\Gamma}(z,\theta,r)>$ is independent of z, and the second term on the left-hand side of Eq. (B1) vanishes.

An analytic solution of Eq. (B1) with $\tilde{\sigma}_V(\theta,\theta')$ given by Eqs. (B2) and (B6) is not available for either of the initial conditions given by Eqs. (B9) and (B10). A numerical algorithm has been devised [B4,B5] based on an iteration or perturbation series. Thus we rewrite Eq. (B1) without the second term, as

$$\frac{d<\hat{\Gamma}(\theta,r)>}{dr} + \frac{k_0}{8\pi}\,[\bar{\sigma}_V(\theta_i)<\hat{\Gamma}(\theta,r) - \tilde{\sigma}_V(\theta,\theta_i)\int <\hat{\Gamma}(\theta',r)>\,d\theta']$$

$$= -\frac{k_0}{8\pi}\,\{[\bar{\sigma}_V(\theta) - \bar{\sigma}_V(\theta_i)]<\hat{\Gamma}(\theta,r)> - \int [\tilde{\sigma}_V(\theta,\theta') - \tilde{\sigma}_V(\theta,\theta_i)]<\hat{\Gamma}(\theta',r)>\,d\theta'\}, \tag{B11}$$

where θ_i is defined by the specification of the initial condition. Setting the right-hand side of Eq. (B11) equal to zero results in a governing equation for which there is an analytic solution for any $\tilde{\sigma}_V(\theta,\theta')$ and any initial condition. The numerical algorithm, then, solves Eq. (B11) in terms of a perturbation series about this analytic solution. We write

$$<\hat{\Gamma}(\theta,r)> = \sum_{n=0}^{\infty} <\hat{\Gamma}_n(\theta,r)>, \tag{B12}$$

where $<\hat{\Gamma}_0(\theta,r)>$ satisfies

$$\frac{d<\hat{\Gamma}_0(\theta,r)>}{dr} + \frac{k_0}{8\pi}\,[\bar{\sigma}_V(\theta_i)<\hat{\Gamma}_0(\theta,r)> - \tilde{\sigma}_V(\theta,\theta_i)\int <\hat{\Gamma}_0(\theta',r)>d\theta'] = 0 \tag{B13}$$

plus the initial condition in Eq. (B10), and $<\hat{\Gamma}_n(\theta,r)>, n \geqslant 1$ satisfies

$$\frac{d<\hat{\Gamma}_n(\theta,r)>}{dr} + \frac{k_0}{8\pi}\,\bar{\sigma}_V(\theta_i)<\hat{\Gamma}_n(\theta,r)>$$

$$= -\frac{k_0}{8\pi}\,\{[\bar{\sigma}_V(\theta) - \bar{\sigma}_V(\theta_i)]<\hat{\Gamma}_{n-1}(\theta,r)> \tag{B14}$$

$$- \int [\tilde{\sigma}_V(\theta,\theta') - \tilde{\sigma}_V(\theta,\theta_i)]<\hat{\Gamma}_{n-1}(\theta',r)>\,d\theta'\},$$

plus homogeneous initial conditions. Equation (B13) is readily solved, and the solution is written

$$<\hat{\Gamma}_0(\theta,r)> = J(\theta) + K(\theta)\ \exp\,(-\rho), \tag{B15}$$

where

$$J(\theta) = \frac{\tilde{\sigma}_V(\theta,\theta_i)I}{\bar{\sigma}_V(\theta_i)}, \tag{B16}$$

$$K(\theta) = <\hat{\Gamma}(\theta,0)> - J(\theta), \tag{B17}$$

and

$$\rho = rk_0\bar{\sigma}_V(\theta_i)/(8\pi). \tag{B18}$$

ρ is a normalized range coordinate. Equation (B14) can next be solved for $<\hat{\Gamma}_n(\theta,r)>$ in terms of $<\hat{\Gamma}_{n-1}(\theta,r)>$. Then, by a sequence of back substitutions we can obtain the following expression for $<\hat{\Gamma}_n(\theta,r)>$ in terms of the funcitons $J(\theta)$ and $K(\theta)$,

$$<\hat{\Gamma}_n(\theta,r)> = T_\theta^n[J(\theta)]\left[1 - \exp(-\rho)\sum_{m=0}^{n-1}\frac{\rho^m}{m!}\right] + T_\theta^n[K(\theta)]\,\frac{\rho^n}{n!}\exp(-\rho). \tag{B19}$$

The notation T_θ^n indicates an n-fold application of the following nonlocal operation defined on the θ coordinate:

$$T_\theta[f(\theta)] = \left[1 - \frac{\bar{\sigma}_V(\theta)}{\bar{\sigma}_V(\theta_i)}\right] f(\theta) + \int \frac{[\tilde{\sigma}_V(\theta,\theta') - \tilde{\sigma}_V(\theta,\theta_i)]}{\bar{\sigma}_V(\theta_i)}\, f(\theta')\, d\theta'. \tag{B20}$$

Equations (B10), (B12), and (B15)-(B20) completely describe the algorithm for a homogeneous background medium and a plane wave source. The convergence of the series can be estimated from consideration of Eqs. (B19) and (B20). For a specified value of ρ, the terms governing the r dependence of $<\hat{\Gamma}_n(\theta,r)>$ fall quite rapidly with increasing n, for $n \geqslant \rho$. Since $\rho = 1$ roughly corresponds to the limit of the single-scatter theory, we might expect values of ρ to be around a few tens but hardly a few hundreds. Also, acting on a function of θ that is sharply peaked around $\theta = \theta_i$ (the case of interest) by the T_θ operator produces a much reduced function (see Eq. (B20)). Both these factors suggest a rapidly converging algorithm which has proven to be true for all trial cases (see the results in Appendix E).

The values of $<\hat{\Gamma}(\theta,r)>$ must be shifted along the θ axis at the transition from one segment to the next so that the peak is at the angle corresponding to the direction of propagation. This models a (discontinuous) change in the direction of the signal as it follows the piecewise-linear approximation of the macroray path.

At higher frequencies the numerical integration may require a finer grid than the default established in the code. Generally, rather than refine the grid, an alternate algorithm is used which is based on an additional approximation that is suitable at higher frequencies. This algorithm is algebraic in nature (see Appendix C).

REFERENCES

B1. L.B. Palmer, D.M. Dundore, B.B. Adams, and J.J. McCoy, "Transverse Horizontal Coherence and Low-Frequency Array Gain Limits in the Deep Ocean," NRL Report 8695, Aug. 1983.

B2. M.J. Beran and J.J. McCoy, "Propagation of Radiation From a Finite Beam or Source Through an Anisotropic Random Medium," *J. Acoust. Soc. Am.* **56**, 1667-1672 (1974).

B3. M.J. Beran, J.J. McCoy, and B.B. Adams, "Effects of a Fluctuating Temperature Field on the Spatial Coherence of Acoustic Signals," NRL Report 7809, May 1975.

B4. J.J. McCoy and M.J. Beran, "Directional Spectral Spreading in Randomly Inhomogeneous Media," *J. Acoust. Soc. Am.* **66**, 1468-1481 (1979).

B5. N. Schwartz and M. J. Beran, "Scattering in an Anisotropic Random Medium: Numerical Calculation," *J. Acoust. Soc. Am.* **65**, 1386-1391 (1979).

Appendix C

HIGH-FREQUENCY (QUASI-ISOTROPIC) ALGORITHM

As the source frequency increases, the algorithm described in Appendix B requires an increasingly finer grid and more iterations. Since COVERT is intended to produce rapid first estimates of coherence loss, an approximation (suitable at higher frequencies) which we have termed a quasi-isotropic approximation is available. The code, as implemented, suggests that this approximation be used when $\alpha > 2.0$.

The details of the quasi-isotropic approximation are discussed in Ref. 3, which is reprinted in Appendix D. The approximation results in the following formulation:

$$<\Gamma(s,r)> = <\Gamma(s,0)> \exp\left\{-\sum_{i=1}^{N}\left[1 - \frac{\bar{\sigma}(s,\theta_i)}{\bar{\sigma}(0,\theta_i)}\right]\left[\frac{R_E(0)}{R_E(\theta_i)}\right]\left[\frac{L_i}{R_E(0)}\right]\right\}, \tag{C1}$$

where N is the number of segments, L_i is the length of the ith segment, θ_i is the angle (measured from horizontal) of the ith segment,

$$R_E(0) = (\epsilon^2 k_0 l_H/2)^{-1}, \tag{C2}$$

$$\frac{R_E(\theta_i)}{R_E(0)} = |\cos\theta_i| + (l_H/l_V)|\sin\theta_i|, \tag{C3}$$

$$\frac{\bar{\sigma}(s,\theta_i)}{\bar{\sigma}(0,\theta_i)} = \frac{l_V|\cos\theta_i| \exp\left[-|s|/(l_V|\cos\theta_i|\right] - l_H|\sin\theta_i| \exp\left[-|s|/(l_H|\sin\theta_i|\right]}{l_V|\cos\theta_i| - l_H|\sin\theta_i|} \tag{C4}$$

ϵ^2 is discussed in Appendix B, and $<\Gamma(s,0)>$ is a description of the source.

$<\Gamma(s,0)>$ should be taken as a constant, but to be consistent with the source required by the low-frequency algorithm, we form $<\Gamma(s,0)>$ by transforming Eq. (B10).

This coherence function (Eq. (C1)) must be transformed to produce the *Total Signal* and *Normalized Scattered Signal* plots discussed in the section entitled **Outputs Calculated**.

Appendix D

REPRINT OF REFERENCE 3

From *J. Acoust. Soc. Am.*, "Directional Spectral Spreading in Randomly Inhomogeneous Media," by John J. McCoy and Mark J. Beran, Copyright©. Used by permission.

Directional spectral spreading in randomly inhomogeneous media

John J. McCoy[a)]

The Catholic University of America, Washington, D.C. 20064

Mark J. Beran[a)]

Tel Aviv University, Ramat Aviv, Israel

(Received 5 September 1978; accepted for publication 4 June 1979)

The redirection of the energy flux in an acoustic signal due to random volume scatter can be described by a radiative transport theory. We consider and compare three such theories, differing one from another in the form of the beam pattern of the incrementally scattered energy, sometimes referred to as an effective scattering cross section. Two of the three theories (termed here quasi-isotropic and highly anisotropic) have already received some attention in the acoustics literature. The third (termed here exact) contains the other two as limiting approximations. The comparison is both analytical and numerical; the numerical phase accomplished for an illustrative acoustic experiment carried out in a canonical environment. The results emphasize the importance of the high anisotropy of the sound-speed fluctuations caused by internal waves on the redirection of energy flux measured in a vertical plane.

PACS numbers: 43.30.Bp, 43.30.Gv

INTRODUCTION

One of the principal consequences of a stochastic volume scattering, e.g., that due to internal waves, is a redirection of the energy flux of an acoustic signal. Thus, this is the source of an added transmission loss as energy is scattered out of the sound channel or a decrease in transmission loss as energy is scattered into shadow zones. Further, it results in degradation in performance of an aperture system, as measured by a decrease in array gain or in the ability to resolve the source of the acoustic signal. Finally, it plays a role in determining the time spreading of an acoustic pulse that arises from the stochastic scatter mechanism.

A theory for predicting the redirection of the energy flux in the acoustic signal is formulated in terms of an averaged directional spectral density. We denote this field measure by $\{\tilde{\Gamma}(\mathbf{x}, \boldsymbol{\theta})\}$, where the braces indicate a statistical (or a temporal) averaging. $\{\tilde{\Gamma}\}$ provides an estimate of the averaged energy flux through an elemental aperture, positioned at $\mathbf{x}$, in an elemental cone of directions, centered about that given by $\boldsymbol{\theta}$. This field measure is related to the mutual coherence function (a two-point correlation function) of the acoustic signal as a Fourier transform pair. We denote the coherence function by $\{\hat{\Gamma}(\mathbf{x}, \mathbf{s})\}$, where $\mathbf{x}$ is the averaged location of the point pair and $\mathbf{s}$ describes the relative locations.

The central importance of $\{\tilde{\Gamma}\}$, or equivalently of $\{\hat{\Gamma}\}$, for discussing propagation experiments has resulted in numerous studies aimed at developing prediction models. The reported models are most commonly formulated in terms of the mutual coherence function; the directional spectral density function, in these models, has the status of a secondary field measure to be determined by transforming the coherence function once it has been determined. In the very recent literature, however, propagation models and scattering (both volume and surface) models formulated directly in terms of $\{\tilde{\Gamma}(\mathbf{x}, \boldsymbol{\theta})\}$ have appeared. The authors can reference a number of studies reported by ourselves[1-4] and a number reported by Tappert and colleagues[5-7] as providing a sampling of these models. The studies by Tappert and colleagues draw quite heavily on the mathematical similarity between the ocean acoustics problem and quantum mechanical theory. Thus, the notation and the terminology favored in them are drawn from quantum mechanics. Our studies, on the other hand, are presented in the context of the physical problem of interest necessitating some, quite trivial, translation if the studies are to be combined.

In the present paper we consider three stochastic volume scatter models formulated in terms of $\{\tilde{\Gamma}(\mathbf{x}, \boldsymbol{\theta})\}$ and discuss their applicability to scattering caused by internal waves. None of the three models are original to this paper, although the authors believe their discussion of the relationships among them is new. Further, the results obtained on applying the models to a typical acoustic experiment envisioned for a realistic ocean environment have not appeared previously. These results shed considerable light on the directional spreading of the energy flux, in the vertical plane, for low-frequency signals (of the order of 100 Hz or less) when the scattering is dominated by internal waves. The results also constitute a reasonable test to apply to the scattering models.

The first of the scattering models is termed "exact" in this paper. The meaning of exact refers to a comparison of the scattering model so designated with the other two models; i.e., they are obtained from the exact model on making additional approximations. In actuality, the exact model contains several approximations, the precise significance of which are just coming to light. The genesis of the exact model lies in some of the earliest studies of stochastic volume scatter, al-

[a)] Consultants of Large Aperture Acoustics Branch, Naval Research Lab, Washington, DC 20375.

 0001-4966/79/111468-14$00.80

though, surprisingly, it first appeared explicitly only recently,[5] and there in the context of a quantum mechanical formulation.

The two approximate models are termed "quasi-isotropic" and "highly anisotropic" since the limitation on their use can be interpreted as a limitation on the degree of anisotropy allowed for the scattering mechanism. As already indicated, each of the approximate models is equivalent to a model that has appeared previously. The quasi-isotropic model, in particular, has a fairly extensive history of use, principally in predicting the scatter of laser beams by atmospheric turbulence,[6,9] but more recently in discussing acoustic signals in the ocean. The highly anisotropic model was derived by us specifically for low-frequency signals and a highly anisotropic ocean.[10] To date, its utility has been limited principally to providing estimates of the directional spreading or the loss of spatial coherence, as measured in a horizontal plane.[11,12]

In Sec. I we present the exact scattering model followed, in Sec. II, by a reduction of this model to the quasi-isotropic and highly anisotropic models. In Sec. III, we introduce the ocean environment and the illustrative experiment and present the results of our numerical calculations. In the Appendices more precise mathematical conditions are placed on the reduction of the exact model to the two approximate models, and on the validity of the exact model itself.

I. A GENERAL SCATTERING MODEL

The volume scatter model is given by the integro-differential equation

$$\frac{d\{\Gamma(\mathbf{x},\boldsymbol{\theta})\}}{ds_\theta} = -\frac{\bar{k}^4}{16\pi^2}\left[\bar{\sigma}_G(\boldsymbol{\theta})\{\tilde{\Gamma}(\mathbf{x},\boldsymbol{\theta})\} - \int \tilde{\sigma}_G(\boldsymbol{\theta},\boldsymbol{\theta}')\{\tilde{\Gamma}(\mathbf{x},\boldsymbol{\theta}')\}d\boldsymbol{\theta}'\right], \tag{1}$$

where

$$\tilde{\sigma}_G(\boldsymbol{\theta},\boldsymbol{\theta}') = \int \sigma(\mathbf{u})\exp[i\bar{k}(\boldsymbol{\theta}-\boldsymbol{\theta}')\cdot\mathbf{u}]d\mathbf{u} \tag{2}$$

and

$$\bar{\sigma}_G(\boldsymbol{\theta}) = \int \tilde{\sigma}_G(\boldsymbol{\theta}',\boldsymbol{\theta})d\boldsymbol{\theta}'. \tag{3}$$

The field measure $\{\tilde{\Gamma}(\mathbf{x},\theta)\}$ is a directional spectral density resolving the averaged power flux through an elemental aperture positioned at $\mathbf{x}$ into flow directions, denoted by $\boldsymbol{\theta}$; a unit normal vector. It is related to the signal coherence function as a Fourier transform pair. Further, $\bar{k}$ is the averaged wavenumber of the narrow-band signal and $\sigma(\mathbf{u})$ is the correlation function of the randomly varying component of $k(\mathbf{x})$, i.e., $\bar{k}\mu_s(\mathbf{x})$,

$$k(\mathbf{x}) = \bar{k}[1+\mu_D(\mathbf{x})+\mu_s(\mathbf{x})], \tag{4}$$

and

$$\sigma(\mathbf{u}) = \{\mu_s(\mathbf{x})\mu_s(\mathbf{x}+\mathbf{u})\}. \tag{5}$$

A brace indicates an ensemble average. The derivative on the left-hand side of Eq. (1) is a substantive derivative taken with respect to distance measured along the ray path passing through the point $\mathbf{x}$ in the direction of $\boldsymbol{\theta}$. For ray paths that make shallow grazing angles with a global principal propagation direction taken to lie along the z axis, the substantive derivative is equated to the partial differential operator,

$$\frac{d}{ds_\theta} \equiv \partial_z + \boldsymbol{\theta}\cdot\nabla_\perp + \tfrac{1}{2}(\nabla_\perp\mu_D)\cdot\nabla_\theta. \tag{6}$$

Here $\nabla_\perp$ and ∇_θ are gradient operators taken with respect to position in a constant range plane z and the two-dimensional directional vector $\boldsymbol{\theta}$, respectively. Also, $\bar{k}\mu_D(\mathbf{x})$ denotes the deterministic, or background, component of the spatially varying wavenumber field. The integral on the right-hand side of Eq. (1) is a directional integral taken over all $\boldsymbol{\theta}'$. The integral in Eq. (2) is a 3-D integral taken over physical space.

The form for the differential operator that constitutes the left-hand side of Eq. (1) is obtained without considering volume scatter.[1] It assumes the validity of a parabolic wave theory together with an additional approximation that we have termed "locally quadratic." The added approximation is identically satisfied for background wavenumbers profiles that are described by functions that are no more complicated than second order. The principal assumption in adding scattering terms to the right-hand side is that processes of diffraction, or refraction, and of scattering are gradual enough that one can neglect any coupling between them over distances that are determined, principally, by the correlation lengths of the scattering mechanism. Tappert and colleagues[5-7] have recognized Eq. (1) to be a special case of a general formalism that is termed a radiative transport theory. (We shall discuss in Appendix A how the locally quadratic assumption may be removed. We also point out in Appendix B that with further work the assumption that refraction effects are not important within a correlation length can probably be corrected.)

In the absence of random volume scatter, the right-hand side of Eq. (1) vanishes, the equation is trivially integrated and the result shows that $\{\tilde{\Gamma}(\mathbf{x},\boldsymbol{\theta})\}$ is a constant along ray paths. This theory differs from the ordinary geometric theory in that there is a continuum of ray paths through each point in the present theory and a finite number of discrete ray paths in the ordinary theory. Further, the acoustic intensity of the ordinary theory is replaced here by $\{\tilde{\Gamma}(\mathbf{x},\boldsymbol{\theta})\}$. The ordinary theory is recovered from the present theory as a limit in which $\{\tilde{\Gamma}(\mathbf{x},\boldsymbol{\theta})\}$ approaches a Dirac dependence on $\boldsymbol{\theta}$. Thus, the ordinary theory can be interpreted as an approximation in which a continuous directional spectrum is replaced by a discrete line spectrum. Since one of the principal effects of random volume scatter, and the effect of interest here, is to cause a spreading of the directional spectrum of acoustic power flux, it is clear that one cannot use the ordinary geometric theory to describe the scattering.

The first of the two scattering terms on the right-hand side of Eq. (1) gives the rate at which power is scattered *from* the ray path through the point $\mathbf{x}$ in the direction $\boldsymbol{\theta}$. The second term gives the rate at which power is scat-

tered *to* this same ray path, i.e., from the remaining ray paths through the point **x**, as given by the directions $\boldsymbol{\theta}'$. The propagation model is energy conservant. Hence, the sum of power scattered from all ray paths passing through **x** equals the sum of power scattered to all ray paths passing through **x**.

While the form of the scattering terms can be obtained by a direct calculation (see, for example, Ref. 5), it is more instructive to argue their validity in an indirect fashion. Thus, we consider first a classical problem of a plane wave incident on a finite scattering volume in an otherwise homogeneous medium. The calculation (a single-scatter calculation) is of the scattered radiation fields, and the quantity calculated is the averaged intensity at a point in the farfield of the scattering volume. The details of the calculation are presented in a number of general treatments (see Ref. 13). The result, which appears to be due to Obukhov (see Ref. 14), shows that the directional distribution of the scattered power flux is related to the correlation function of the randomly varying refractive index field as a Fourier transform pair.

Referring to Eq. (1), the second term on the right-hand side provides the directional redistribution, in $\boldsymbol{\theta}$, of the power scattered from the incident directions $\boldsymbol{\theta}'$. For plane-wave incidence $\{\tilde{\Gamma}(\mathbf{x}, \boldsymbol{\theta}')\}$ has a Dirac dependence on $\boldsymbol{\theta}'$. Hence, $\tilde{\sigma}_G(\boldsymbol{\theta}, \boldsymbol{\theta}')$ is properly interpreted as a beam pattern for the scattered power flux. Consistent with the classical result discussed above, it is clear that $\tilde{\sigma}_G$ must be related to $\sigma(\mathbf{u})$, the refractive index correlation function, as a Fourier transform pair. With this fact accepted, the first term is a necessity required by energy conservation. Thus, the only feature of Eq. (1) that requires any comment beyond that provided by Obukhov in 1941 is possibly the constant coefficient $\bar{k}^4/16\pi^2$. To obtain this requires a somewhat more detailed analysis.

With the validity of the general scattering model established, we can address ourselves to the development of other approximate scattering models that can be obtained from Eq. (1) on making additional assumptions. In the next section we consider two such approximate models and their relationships to the general model.

II. A QUASI-ISOTROPIC AND A HIGHLY ANISOTROPIC SCATTERING MODEL

In this section we consider the kernel function of the scattering integral and introduce two sets of different approximations that lead to two different reduced scattering models.

First we consider the following interpretation of Eq. (2). The unit vector

$$\bar{\boldsymbol{\theta}} = (\boldsymbol{\theta} + \boldsymbol{\theta}')/|\boldsymbol{\theta} + \boldsymbol{\theta}'| \tag{7}$$

gives a direction that is orthogonal to the vector $\boldsymbol{\theta} - \boldsymbol{\theta}'$. This suggests that we write Eq. (2) as

$$\tilde{\sigma}_G(\boldsymbol{\theta}, \boldsymbol{\theta}') = \int_{\mathbf{u}_T} \left(\int \sigma(\mathbf{u}_T, \mathbf{u}_{\bar{\theta}}) du_{\bar{\theta}} \right) \exp[i\bar{k}(\boldsymbol{\theta} - \boldsymbol{\theta}') \cdot \mathbf{u}_T] d\mathbf{u}_T, \tag{8}$$

where $\mathbf{u}_{\bar{\theta}}$ is measured along the $\bar{\boldsymbol{\theta}}$ direction and $\mathbf{u}_T$ is orthogonal to it. Now, if we choose to locate $\boldsymbol{\theta}, \boldsymbol{\theta}'$ relative to $\bar{\boldsymbol{\theta}}$ by planar angles (θ_x, θ_y), and (θ_x', θ_y'), which we assume to be small enough to replace $\sin\theta = \tan\theta = \theta$, then we can write the following scalar form for Eq. (8):

$$\tilde{\sigma}_G(\boldsymbol{\theta}, \boldsymbol{\theta}') = \int \int \left(\int \sigma(u_x, u_y, u_{\bar{\theta}}) du_{\bar{\theta}} \right) \times \exp(i\bar{k}[(\theta_x - \theta_x')u_x (\theta_y - \theta_y')u_y]) du_x du_y, \tag{9}$$

where u_x, u_y are measured along lines orthogonal to $\bar{\boldsymbol{\theta}}$. We note that the only approximation introduced in writing Eq. (9), beyond those already contained in the general model, restricts the scattering angles to be narrow enough that we can approximate the trigonometric functions as indicated.

Although Eq. (9) gives the appearance of a scattering integral being a convolution, it is not. That it is not a convolution is seen with the realization that the reference direction for measuring the angles (θ_x, θ_y), and (θ_x', θ_y') depends on the absolute directions defined by $\boldsymbol{\theta}$ and $\boldsymbol{\theta}'$. For isotropic statistics, of course, one can replace, with no additional assumption, the averaged direction $\bar{\boldsymbol{\theta}}$ with "any" direction, say $\boldsymbol{\theta}^*$. This last direction is to be taken to be the same for all $\boldsymbol{\theta}'$ in the scattering integral. Hence, the scattering integral is, in this case, a convolution.

This same reasoning, which is exact for an isotropic medium, can be argued to be approximate for a quasi-isotropic medium. The condition is that the range of significant $\boldsymbol{\theta}$ and $\boldsymbol{\theta}'$ directions is sufficiently narrow that one can replace $\bar{\boldsymbol{\theta}}$ with a $\boldsymbol{\theta}^*$, which is independent of $\boldsymbol{\theta}$ and $\boldsymbol{\theta}'$. A mathematical statement of the condition of validity, then, depends on the angular spectral width of the signal, the absolute direction of the principal energy flux, and the degree of anisotropy of the medium. Since the spectral width of the acoustic signal decreases with increasing frequency, the approximation termed quasi-isotropic might also be interpreted as a high-frequency approximation. In the Appendices the condition for the validity of the approximation is made more precise by identifying the required large number.

A scattering model that has received much attention in the optics literature is expressed in terms of the mutual coherence function as measured at two points on the same range plane, z. We denote the coherence function by $\{\hat{\Gamma}(\mathbf{x}_{\perp_1}, \mathbf{x}_{\perp_2}, z)\}$ and write (cf. Refs. 13, 15)

$$\partial_z\{\hat{\Gamma}\} - \frac{i}{2\bar{k}}(\nabla_{\perp_1}^2 - \nabla_{\perp_2}^2)\{\hat{\Gamma}\} - \frac{i\bar{k}}{2}[\mu_D(\mathbf{x}_{\perp_1}, z) - \mu_{\bar{D}}(\mathbf{x}_{\perp_2}, z)]\{\hat{\Gamma}\} = -\bar{k}^2[\bar{\sigma}(0) - \bar{\sigma}(\mathbf{x}_{\perp_1} - \mathbf{x}_{\perp_2})]\{\hat{\Gamma}(\mathbf{x}_{\perp_1}, \mathbf{x}_{\perp_2}, z)\}, \tag{10}$$

where

$$\bar{\sigma}(\mathbf{x}_{\perp_1} - \mathbf{x}_{\perp_2}) = \frac{1}{4}\int_{-\infty}^{\infty} \sigma(\mathbf{x}_{\perp_1} - \mathbf{x}_{\perp_2}, u_z) du_z, \tag{11}$$

and $\nabla_\perp^2$ denotes a two-dimensional Laplacian operator. To obtain a model expressed in terms of $\{\tilde{\Gamma}(\mathbf{x}, \boldsymbol{\theta})\}$ from Eq. (11), we first transform to average and difference coordinates, introduce the locally quadratic approximation that replaces the difference in μ_D values with a dif-

ferential expression, and then Fourier transform the difference coordinate. The result is exactly that obtained from our quasi-isotropic scattering model if we (1) restrict all ray paths to make narrow angles with the horizontal and (2) identify $\boldsymbol{\theta}^*$ with $\mathbf{e}_z$, a unit vector in the range direction. The first restriction is acceptable in many optical experiments, since refraction by an inhomogeneous background medium is often not a factor; the identification of $\boldsymbol{\theta}^*$ with $\mathbf{e}_z$ represents no additional approximation since the scattering mechanism of importance is isotropic.

Recently, the quasi-isotropic model has been suggested for ocean acoustic experiments.[16] A degree of anisotropy is allowed in this suggestion, since $\boldsymbol{\theta}^*$ is taken to vary with position along a deterministic multipath. However, it is important to note that the degree of anisotropy is limited. (Actually an additional assumption is made in these last-mentioned studies, which appears to limit the rate of curvature of the ray paths. For straight ray paths, Eq. (10) can be solved in closed form.)

Because of the quasi-isotropic nature of the above discussed model, it is not applicable for lower frequency ocean acoustic experiments. The scattering mechanism in the ocean is highly anisotropic. For this reason, the present authors suggested a second approximate model, which might be termed highly anisotropic.[10] In effect, the highly anisotropic medium approximation uses the formal approximation

$$\sigma(\mathbf{u}) = \left(\int \sigma(\mathbf{u}_H, u_y') du_y' \right) \delta(u_y) , \tag{12}$$

where u_y is measured along the depth direction and $\mathbf{u}_H$ lies in a horizontal plane. The condition for the valid use of Eq. (12) is that the largest correlation length measured along the depth direction is small compared to a projected wavelength. A more precise condition can be written as

$$\bar{k} l_v \bar{\theta} \ll 1 , \tag{13}$$

where l_v is the largest vertical correlation length. This condition is discussed further in the Appendices, where it is shown that the quasi-isotropic and highly anisotropic approximations represent two limits of a continuum of anisotropy measures.

With Eq. (12), Eq. (2) becomes

$$\tilde{\sigma}_G(\boldsymbol{\theta}, \boldsymbol{\theta}') = \int \left(\int \sigma(\mathbf{u}_H, u_y) du_y \right) \exp[i\bar{k}(\boldsymbol{\theta} - \boldsymbol{\theta}') \cdot \mathbf{u}_H] d\mathbf{u}_H . \tag{14}$$

To reduce Eq. (14) to a scalar form, we introduce planar angles locating $\boldsymbol{\theta}, \boldsymbol{\theta}'$ relative to a horizontal reference direction, which we denote by $\bar{\boldsymbol{\theta}}_H$. Using (θ_x, θ_y), (θ_x', θ_y') to again denote the planar angles and assuming them to be small enough to approximate $\sin\theta = \tan\theta = \theta$ and $\cos\theta = 1 - \frac{1}{2}\theta^2$, Eq. (14) leads to

$$\begin{aligned} &\tilde{\sigma}_G(\theta_x - \theta_x'; \theta_y, \theta_y') \\ &= \int \int \left(\int \sigma(u_x, u_y, u_z) du_y \right) \\ &\quad \times \exp\left(i\bar{k} \left[(\theta_x - \theta_x') u_x - \frac{1}{2} (\theta_y^2 - \theta_y'^2) u_z \right] \right) du_x \, du_z \end{aligned} \tag{15}$$

where u_z, u_x are measured along horizontal lines in the $\mathbf{u}_H$ direction and normal to this direction, respectively.

Like the quasi-isotropic model, our highly anisotropic model[10] was originally expressed in terms of $\{\hat{\Gamma}(\mathbf{x}_{\perp_1}, \mathbf{x}_{\perp_2}, z)\}$ and was restricted to ray paths that make small angles relative to the horizontal. To obtain the model expressed in terms of $\{\tilde{\Gamma}(\mathbf{x}, \boldsymbol{\theta})\}$, as presented here, we need, first to transform to average and difference coordinates and then to Fourier transform the difference coordinate. The result is seen to be identical to Eq. (15).

Two questions relative to the quasi-isotropic and highly anisotropic models are in order: (1) Why introduce them at all? (2) Can they be justified for a realistic ocean acoustic experiment? The answer to the first is that for some limited experiments one can, by making still additional assumptions, go much further toward obtaining simple closed-form expressions for quantities of experimental interest, if one can justify the simpler models. For example, the authors were able to obtain an algebraic expression giving the horizontal coherence of a received signal in terms of the signal frequency, the range of the experiment, and a single environmental parameter.[11,12] We obtained the result:

$$\{\hat{\Gamma}(z, x)\} = \hat{I}_0 \exp[-E(\bar{k}x)^{3/2}(\bar{k}z)] . \tag{16}$$

Here, z is the range variable and x is the horizontal separation—both dimensional variables; $\bar{k}$ is the signal wavenumber; and E is a single nondimensional environmental parameter. This simple expression has been used successfully to explain the results of a number of sea experiments carried out by Moseley and colleagues at the Naval Research Laboratory (see Ref. 17).

To answer the second question requires that we compare (numerically) predictions made by the approximate models with those made by the more general model, which they approximate. In the next section, then, we present such comparisons for some experiments of interest.

III. NUMERICAL COMPARISON OF SCATTERING MODELS

The scattering models differ from one another in the predicted rate at which energy is scattered, as measured by an "extinction" coefficient, and in the beam pattern of the locally scattered energy, sometimes referred to as an effective scattering cross section. (This notation might be somewhat unfortunate, since the function has been normalized. In radiative transport theory the nondimensionalized scattering cross section is sometimes referred to as a phase function, but this terminology would probably result in even more confusion.) Appropriate numerical measures of these parameters are $\bar{\sigma}_G(\boldsymbol{\theta})$ and $\tilde{\sigma}_G(\boldsymbol{\theta}, \boldsymbol{\theta}')$, respectively. Thus, we consider sample calculations for these functions for an illustrative ocean acoustic experiment. We would caution against applying the numerical results of this section to a realistic ocean acoustic experiment. To study the real ocean, it would be necessary to solve Eq. (1). Our purpose in presenting these numbers is not to reproduce a realistic experiment; it is to illustrate the differences between the scattering terms of the three models. Re-

fraction effects, while being extremely important in matching data from a realistic sea test, are not at issue here since all three models can accommodate refraction.

First, we need describe the fluctuating refractive index field, which we do by assuming the correlation function

$$\sigma(\mathbf{u}) = \epsilon^2 \exp\left[-\left(\frac{|u_v|}{l_v} + \frac{|\mathbf{u}_H|}{l_H}\right)\right]; \tag{17}$$

l_v and l_H are characteristic dimensions of the sound-speed fluctuations as measured along a vertical and a horizontal line, respectively, and ϵ^2 depends on the strength of the fluctuations. This correlation function gives a one-dimensional refractive index fluctuations spectrum that falls off, with decreasing size scale, according to a minus-two law. [It has this behavior for size scales that are small when compared to l_v (vertical measurements) or l_H (horizontal measurements).] There would appear to be a quite general agreement among oceanographers that a minus-two power law is the best single power law for describing fluctuations on length scales that are of the order of tens of meters measured along a vertical line and of kilometers measured along a horizontal line. Experience indicates that it is the length scales in this range that dominate the acoustic experiments of interest, i.e., frequencies of the order of several tens to a couple of hundred Hertz and ranges of from some hundred to several thousands of kilometers. There would be considerably less agreement as to specific numbers for l_v and l_H. The numbers that we shall use are $l_v = 100$ m and $l_H = 7000$ m. Although the choices are somewhat arbitrary, the anisotropy ratio of 70:1 falls within the one to two orders of magnitude that appears to be an accepted rule of thumb. Further, the 7000 m figure appears to be quite reasonable to a number of oceanographers; although the 100 m figure is a bit large. [The figures $l_H = 7000$ m and $l_v = 100$ m are argued by the JASON group (see Refs. 18, 19) as being the most representative of the ocean. Our own reading of oceanographic data would indicate that the simple exponential with $l_v = 100$ m predicts more energy at the larger length scales than can be justified. For purposes of illustration, however, we accept their

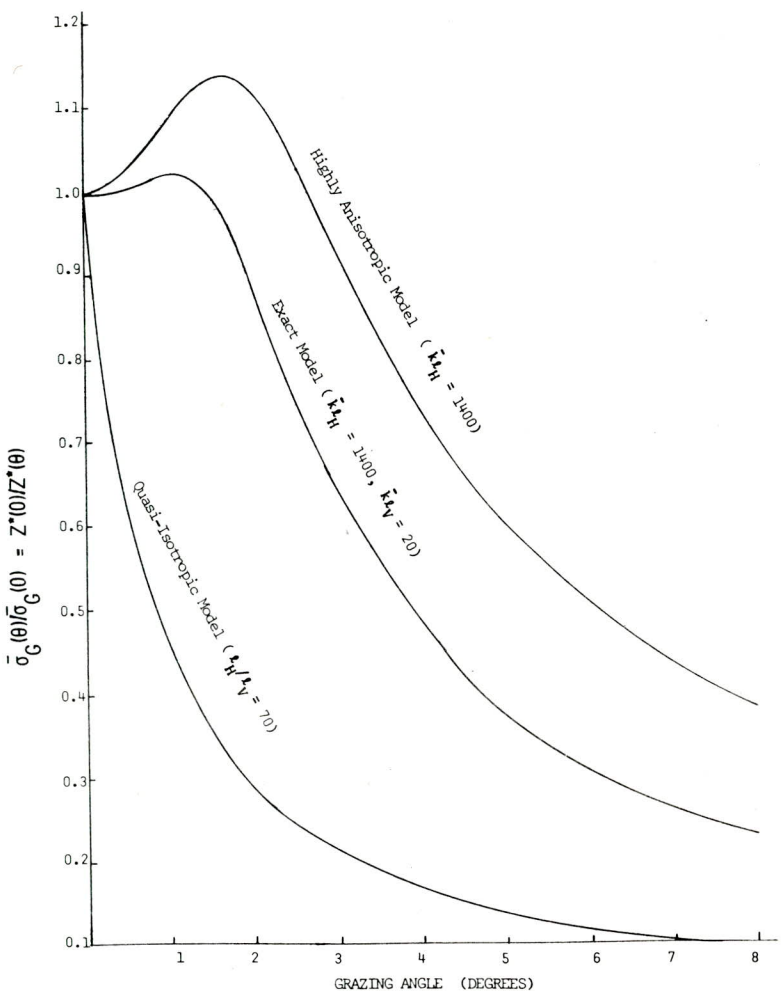

FIG. 1. Dependence of rate of energy scatter on grazing angle of incident signal.

values.] The difficulty is undoubtedly caused by an oversimplification of our description of the phenomenon mandated by our desire to obtain easily handled, albeit realistic, analytic forms. Assigning a single number to ϵ^2 is even more problematical than for l_v and l_H. Measured data would support values that range over several orders of magnitude, say 10^{-4} to 10^{-7}, depending on location in the water column. Since the principal effect of the value of ϵ^2 is to set a scale for measuring range, however, the specific value is not of great import in our discussion. Thus, we simply absorb ϵ^2 in $\bar{\sigma}_G(\theta)$ and choose the value of $1/\bar{\sigma}_G(0)$, where 0 denotes a horizontally directed line, to normalize the range variable. A range value of unity, then, would correspond to the range at which some significant percentage, say half, of the energy in a horizontally directed incident signal has been scattered. It is to be noted that the normalization range is different, as predicted by the three theories; although, for the cases investigated the values were all of the same order of magnitude.

In order to specify $\bar{\sigma}_G(\theta)/\bar{\sigma}_G(0)$ and $\tilde{\sigma}_G(\theta,\theta')/\bar{\sigma}_G(\theta',\theta')$ completely, we need also prescribe the frequency of the signal. We choose a frequency of 50 Hz since this value is fairly typical of the values usually discussed in the context of long-range signal propagation.

For the choice of values used, we find that the parameter $\alpha = kl_v^2/l_H = 0.3$. In Appendix C we point out that if $\alpha \gg 1$, we expect the quasi-isotropic approximation to be valid; while if $\alpha \ll 1$, we expect the highly anisotropic model to yield good results. Since $\alpha = 0.3$ our expectation is that neither approximation will give very good results, but that the highly anisotropic approximation will be the more satisfactory.

In Fig. 1 we illustrate the dependence of the rate at which energy is scattered on the grazing angle made by the incident signal and a horizontal line. Since the refractive index fluctuations are azimuthally isotropic, there is no dependence of energy scatter rate on azimuthal direction. Of greatest physical significance is the very strong dependence of the scattering rate on vertical direction. All other considerations being equal, the scattering will be strongest in regions in which the ray paths are horizontal, with a marked decrease in scattering strength as the grazing angle increases. Of lesser physical significance, although of interest, are the shapes of the curves as predicted by the three theories. Notice that the quasi-isotropic model can incorporate some degree of anisotropy, but this is only because we have chosen to introduce the idea of a local principal propagation direction. In one common derivation of the quasi-isotropic model,[13] the assumption made is interpreted as a delta function behavior for the correlation function with separation distance measured in the range direction. If the range direction in this statement is interpreted as a global direction, there would be no way to incorporate the behavior illustrated in Fig. 1 for a principal ray path that is curved.

The beam patterns of the locally scattered energy likewise will depend on the vertical grazing angle. Illustrated in Fig. 2 are vertical sections of these local beam patterns for incident grazing angles of 0°, 2°, and 5°. The

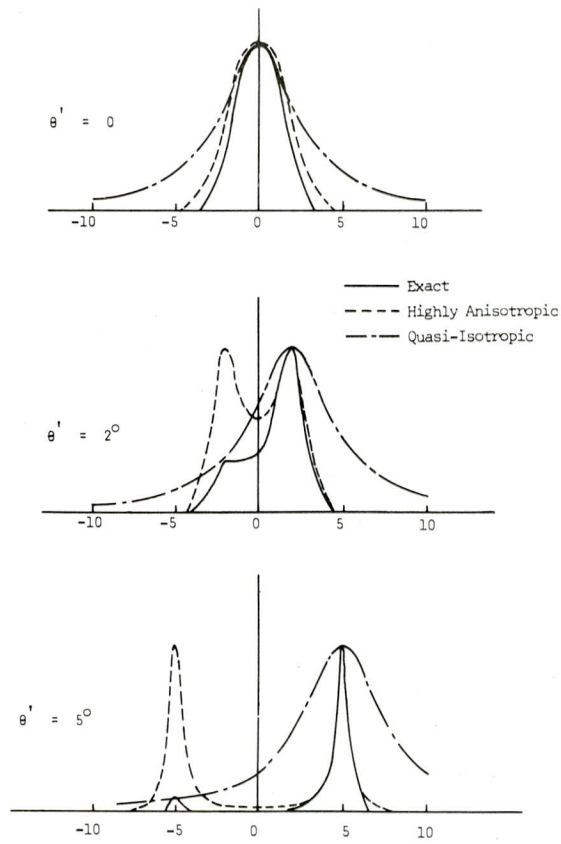

FIG. 2. The effective scattering cross section according to three models (exponential correlation function; $l_H = 7000$ m, $l_v = 100$ m, $f = 50$ Hz).

quasi-isotropic beam patterns are the easiest to describe since they are always symmetrically distributed about the incident direction, a concomitant of the scattering integral being a convolution. Further, there is very little dependence of the width of the beam pattern on grazing angle. A good estimate of the width, as measured by the 3-dB value, is given by $(\bar{k}l_v)^{-1}$. The highly anisotropic beam patterns are next easiest to describe. For 0° incidence the beam pattern has much the same shape as for the quasi-isotropic model, but is somewhat narrower. An estimate of the width is given by $(\bar{k}l_H)^{-1/2}$. For other than 0° grazing angle, the highly anisotropic beam patterns are no longer symmetric about the incident direction; they are, in fact, always symmetric about the horizontal line. Further, the beam patterns exhibit a two-lobed structure that becomes more pronounced with increasing grazing angle. Finally, the width of the individual lobes noticeably decreases with increasing grazing angle. An estimate of the individual lobe width is given by $(\bar{k}l_H\theta')^{-1}$ for $\theta' \geq (\bar{k}l_H)^{-1/2}$. The marked decrease in the width of the scattering cross section with increasing grazing angle is of interest since it suggests the possibility of a saturation of sorts when discussing the directional spectral spreading as measured in the vertical plane. Thus, a signal that is

initially horizontal will spread according to the 0° beam pattern, a comparatively wide beam pattern. The subsequent scatterings of the energy flowing in directions at the extremities of this 0° beam pattern are governed by different beam patterns, however, and these new beam patterns tend to be far more restrictive as far as the further spreading of the signal is concerned. Thus, the existence of a saturation is possible. It is noteworthy that the quasi-isotropic model does not contain this phenomenon.

To understand the "exact" effective scattering cross sections, it is easiest to interpret the directional redistribution of energy flux due to scattering as a filtering process. Then, the exact filter can be interpreted as two filters applied in sequence. One filter is accurately described by the quasi-isotropic model, and the second by the highly anisotropic model. This is clearly demonstrated by the graphical illustrations. The exact beam patterns exhibit the tendency to a two-lobed structure with increasing grazing angle. Now, however, the effect of the quasi-isotropic filter is a tendency to suppress one of the lobes, with the degree of suppression increasing with incident grazing angle. Finally, the strong dependence of the width of a single lobe on grazing angle, predicted by the strongly anisotropic model, is also predicted by the exact model. Thus, the possibility of a saturation of sorts exists for this model, too.

There are far less dramatic differences in the horizontal sections of the local beam patterns; hence, we do not present any illustrative graphs. In each instance the patterns are symmetric about the incident signal direction; in shape they are all like the 0° patterns of Fig. 2. The beam widths of all are of the order of $(\bar{k}l_H)^{-1}$, although the coefficient of this parameter depends on the scattering model and on the incident signal direction as measured in the vertical plane. The last-mentioned dependency is the cause of a coupling between the vertical spectral spreading of a signal and the subsequent azimuthal spreading.

Figures 1 and 2 illustrates only the behavior of the model parameters. To illustrate differences in predicted results for specific acoustic experiments, we need apply the models to "typical" cases. For the cases treated the background medium was chosen to be homogeneous, i.e., $\mu_0 \equiv 0$, and the incident signal was taken to be a plane wave. (Actually we allowed, for computational purposes, some small, but finite, directional spectral width of the incident signal.) Again the frequency was taken to be 50 Hz. The results are shown in Figs. 3–11. To explain the graphs we first note that we only considered spreading in the vertical plane, i.e., that which would be measured by a vertical line array. Now, the received beam pattern will consist of two components: the first, a replica of the incident signal with somewhat lower power content, and the second, the scattered signal. Since the models are all energy conservant the sum power of the two components in all cases remains a constant. There is, however, a monotonic transfer of power content with increasing range from the unscattered portion of the total signal to the scattered portion. In addition to increasing in strength, the width of scattered signal increases with range. Our primary interest is with the growth in width of the scattered signal. Accordingly, we first subtracted from the total signal that portion that had not been scattered (i.e.,

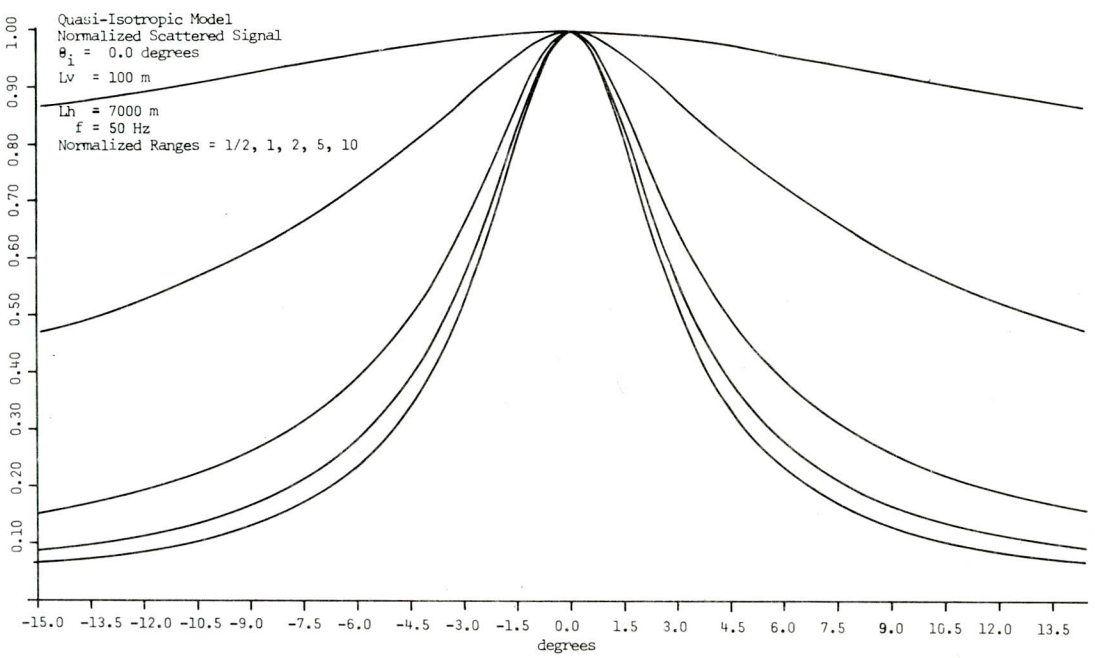

FIG. 3. Directional dependence of the normalized scattered signals according to one of the models. (Specific model and conditions of experiment illustrated on figure proper.)

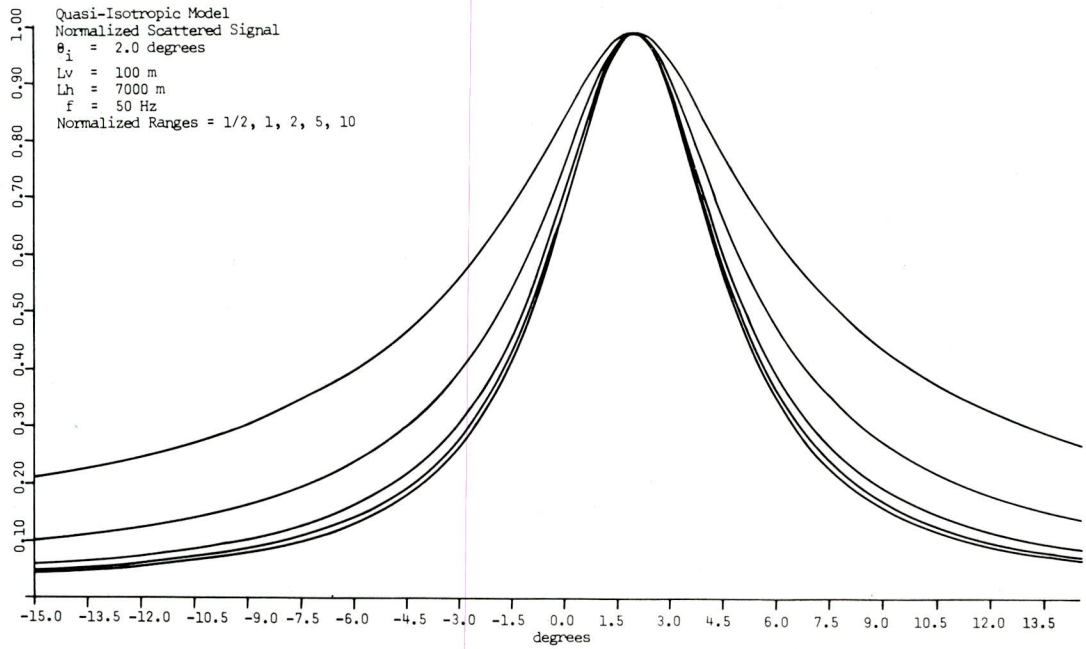

FIG. 4. Directional dependence of the normalized scattered signals according to one of the models. (Specific model and conditions of experiment illustrated on figure proper.)

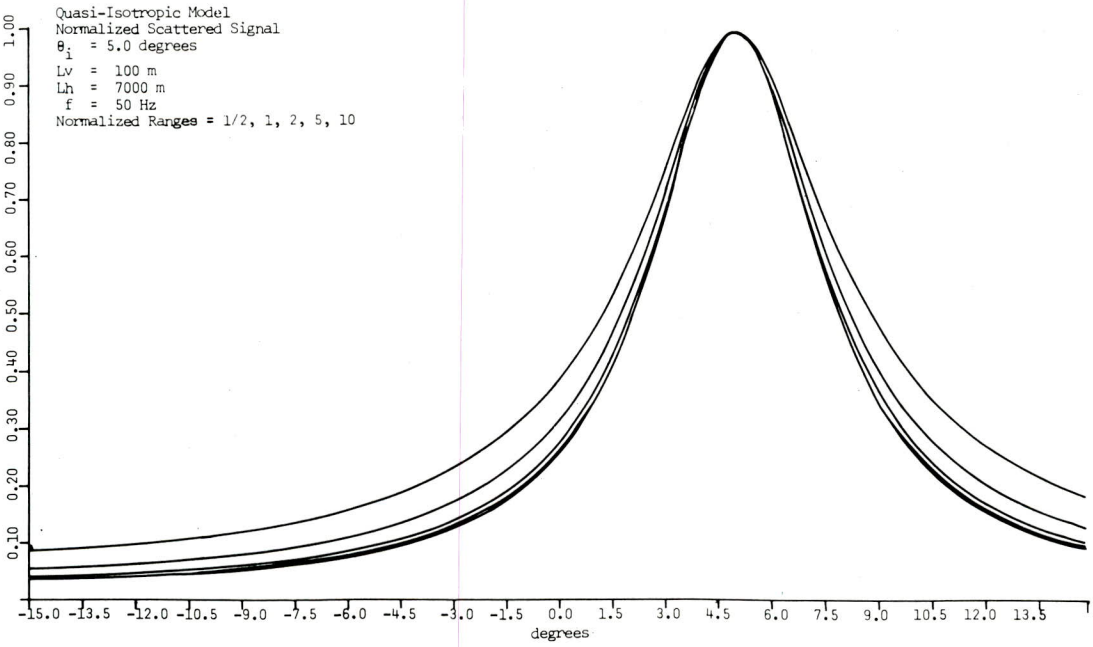

FIG. 5. Directional dependence of the normalized scattered signals according to one of the models. (Specific model and conditions of experiment illustrated on figure proper.)

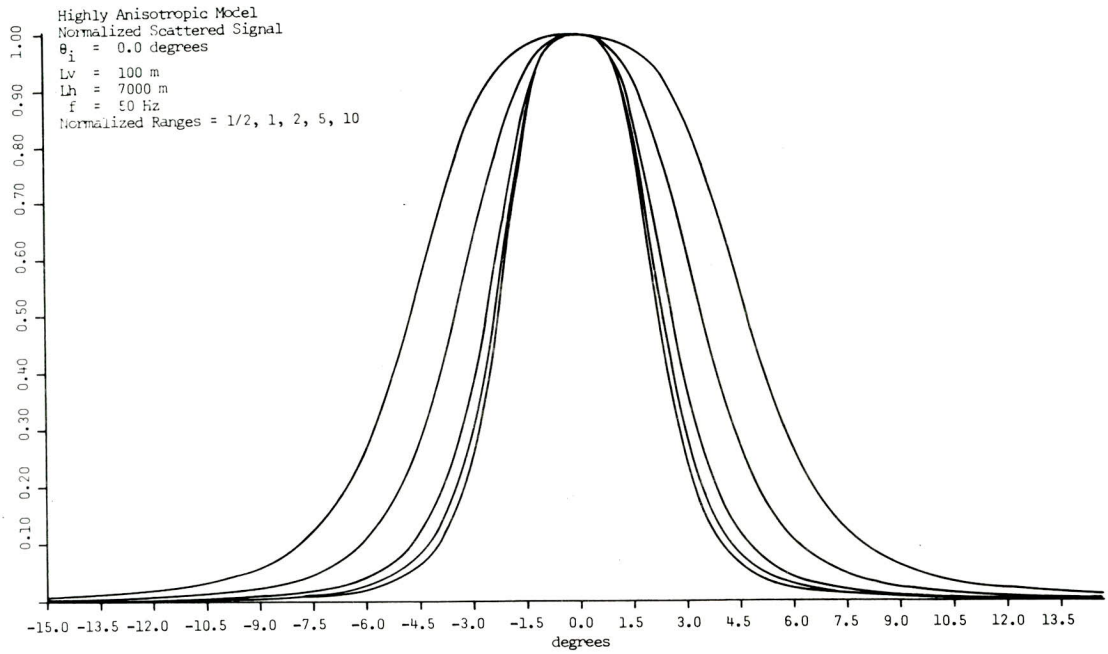

FIG. 6. Directional dependence of the normalized scattered signals according to one of the models. (Specific model and conditions of experiment illustrated on figure proper.)

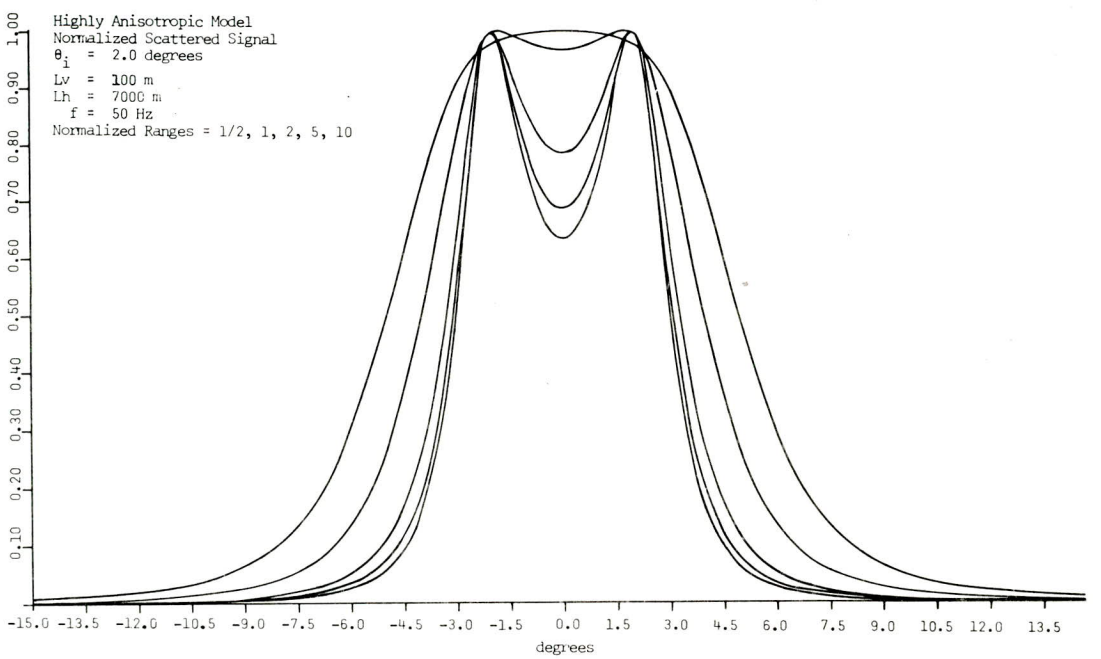

FIG. 7. Directional dependence of the normalized scattered signals according to one of the models. (Specific model and conditions of experiment illustrated on figure proper.)

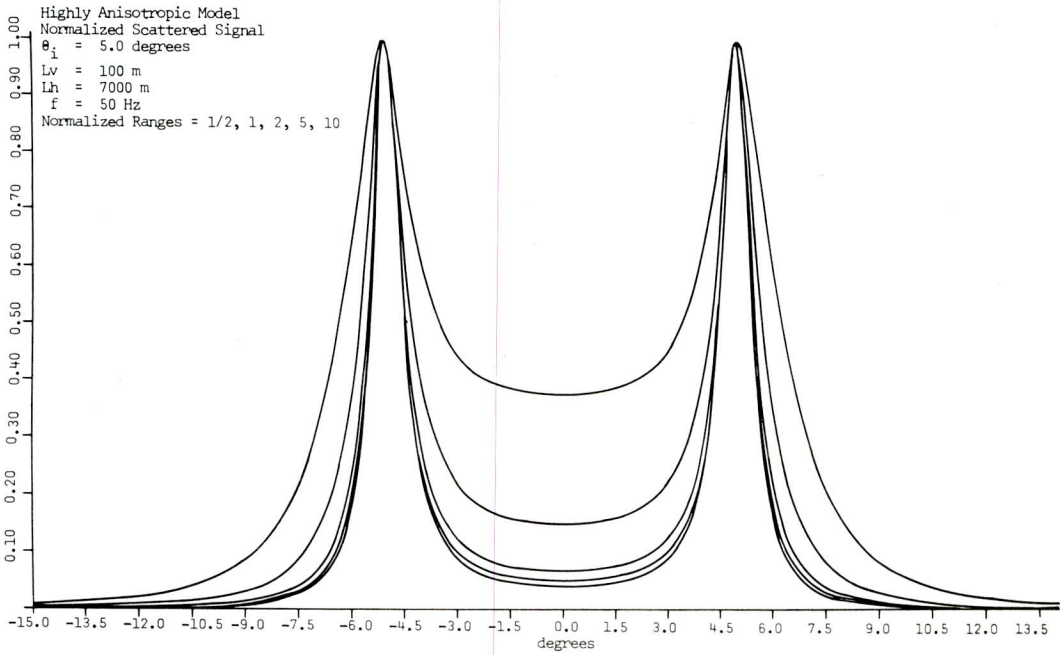

FIG. 8. Directional dependence of the normalized scattered signals according to one of the models. (Specific model and conditions of experiment illustrated on figure proper.)

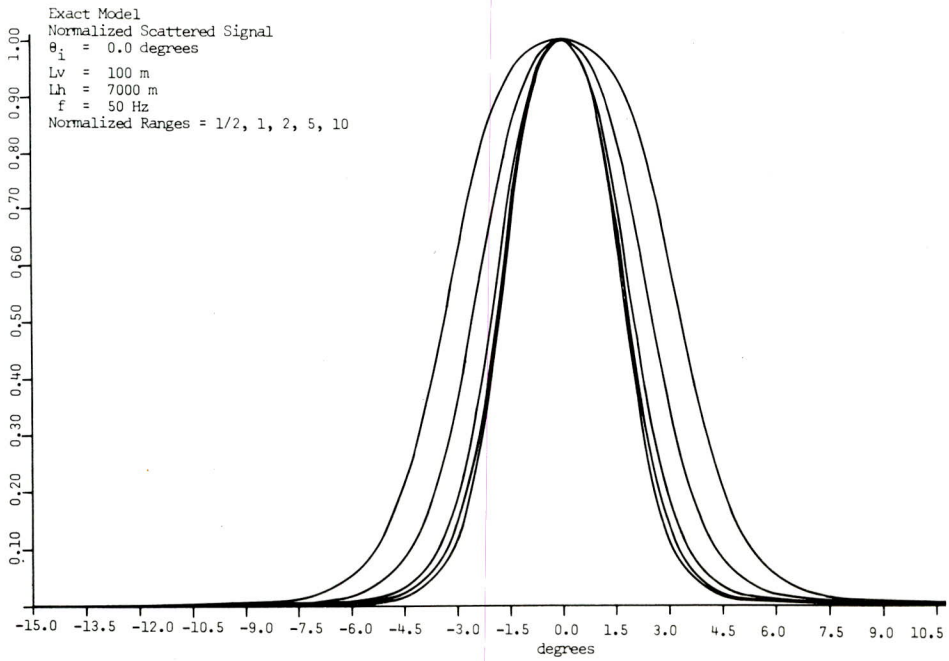

FIG. 9. Directional dependence of the normalized scattered signals according to one of the models. (Specific model and conditions of experiment illustrated on figure proper.)

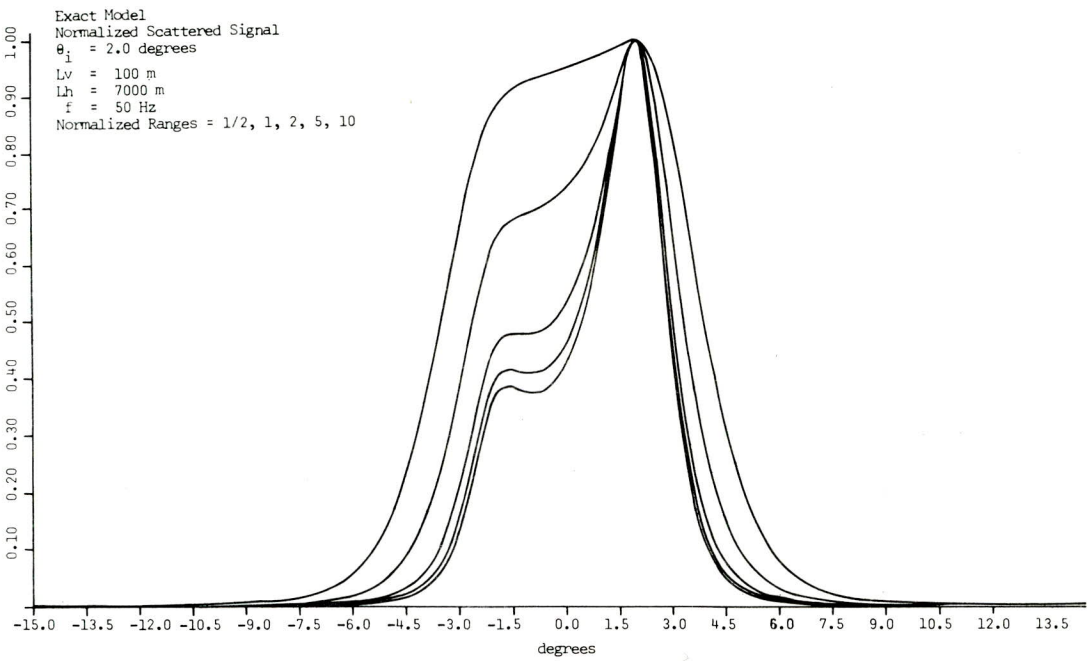

FIG. 10. Directional dependence of the normalized scattered signals according to one of the models. (Specific model and conditions of experiment illustrated on figure proper.)

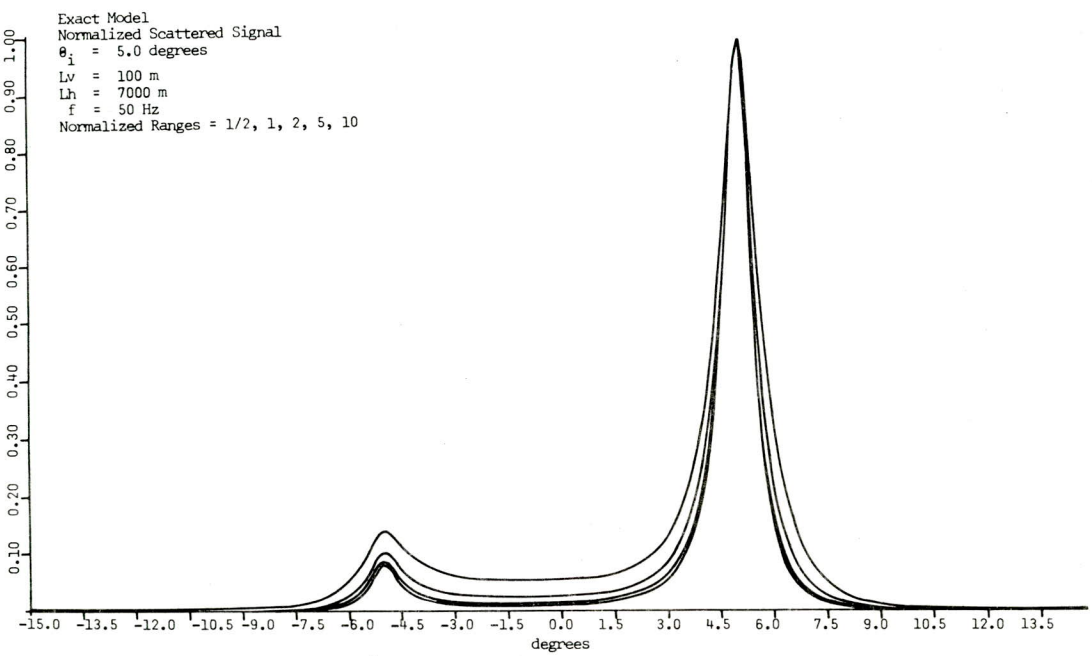

FIG. 11. Directional dependence of the normalized scattered signals according to one of the models. (Specific model and conditions of experiment illustrated on figure proper.)

the replica of the incident signal) and subsequently renormalized the result to have a maximum value of unity. The nine graphs consist of the results of the three models for three initial grazing angles: $0°, 2°, 5°$. The ranges are $Z = \frac{1}{2}, 1, 2, 5, 10$, where the meaning of $Z = 1$ has been discussed. Thus, $Z = \frac{1}{2}$ is in the single scatter region and the scattered beam patterns will be shaped much like $\bar{\sigma}_G(\theta, \theta')$, as in Fig. 2. The range $Z = 10$ is nominally far into the multiple-scatter region and little energy is expected to be still in the unscattered signal.

The graphs are largely self-explanatory, although some features warrant some emphasis. First, the quasi-isotropic model predicts beam widths that quickly exceed those for which the parabolic theory is valid. This would indicate a paradox that would be quite difficult to resolve should this model be accurate. Fortunately, it is not as is readily seen by comparing the results of this model with those of the exact model. Also, referring to the quasi-isotropic model results, we note an apparent decrease in the rate of spreading of the scattered beam pattern with increasing grazing angle. This is due entirely to the decrease in scattering rate with increasing grazing and not to a decrease in the effective scattering cross section.

The two-lobed structure for the scattered signal predicted for the highly anisotropic model is clearly visible for $Z \lesssim 1$. Subsequent scatterings, however, tend to fill out the region about $\theta = 0°$, as might be expected. The speculation that the directional spectral spreading in the vertical plane should tend to a quasi-steady state is not yet borne out by the graphs for $Z < 10$. The reason for this is that the vertical spreading does not, in fact, actually saturate, but tends to a growth rate that is significantly slower than the initial growth rate.[20,21] This slower growth rate represents a quasi-steady state on graphs for which the characteristic angular spread is plotted as a function of propagation distance. Our manner of presenting results, subtracting out the unscattered signal and renormalizing the remainder, emphasizes, on the other hand, continuing growth. For $Z > 10$ ($Z = 20$, 30), the growth rate will be slower than at $Z = 10$.

The results using the exact model are easily interpreted in the light of the preceding discussions. The most noteworthy conclusion to be drawn from these is that like the highly anisotropic model, the exact model predicts a loss of signal coherence with separation distance measured along a vertically positioned line array that would be much less than a similar prediction that is based on the quasi-isotropic model.

IV. CONCLUDING REMARKS

In this paper we have considered three random volume scatter models that might all be classed as radiative transport theories. The models differ from each other in the analytic forms chosen for the scattering kernel. The models were termed exact, quasi-isotropic, and highly anisotropic, with the latter two being limiting cases of the first depending on the degree of anisotropy of the scattering mechanism. Each model can incorporate an inhomogeneous background sound-speed profile, a degree of inhomogeneity in the statistics of the refractive index fluctuations, and a finite source. To do so, however, one would most certainly require the use of efficient numerical codes. It is our belief that such codes should be based on the exact model, since using either of the two limiting approximations would appear to provide little computational advantage.

The approximate models are of interest, however, since they can lead to analytic solutions in special situations. These solutions can provide simple algebraic expressions useful for obtaining first order estimates of parameters of interest to a systems designer. As an example, we cited a special case solution based on the highly anisotropic model that allows one to estimate the loss of coherence as measured along a horizontal line array positioned transverse to the principal signal direction. Because of this interest in the approximate scattering theories, it is important to consider their relationship to the more exact model. This was the purpose of the present paper.

ACKNOWLEDGMENTS

The computer programming was accomplished by Janet Mason. The authors acknowledge with appreciation this effort. We also thank Ralph N. Baer for discussions on the implementation of the numerical codes.

APPENDIX A: VALIDITY OF EQ. (6)

In the absence of scattering the coherence function $\{\hat{\Gamma}(\mathbf{x}_{\perp_1}, \mathbf{x}_{\perp_2}, z)\}$ obeys the equation

$$\left(\frac{\partial}{\partial z} - \frac{i}{2k}(\nabla_{\perp_1}^2 - \nabla_{\perp_2}^2) - \frac{ik}{2}[\mu_D(\mathbf{x}_{\perp_1}) - \mu_D(\mathbf{x}_{\perp_2})]\right)\{\hat{\Gamma}\} = 0. \quad \text{(A1)}$$

The only approximation in this equation is that the pressure is governed by the parabolic equation. For simplicity we assume that the speed of sound profile varies only in the transverse direction.

In terms of the sum and difference coordinates

$$\mathbf{x}_\perp = \tfrac{1}{2}(\mathbf{x}_{\perp_1} + \mathbf{x}_{\perp_2}), \quad \mathbf{s} = \mathbf{x}_{\perp_1} - \mathbf{x}_{\perp_2},$$

Eq. (A1) becomes

$$\left(\frac{\partial}{\partial z} - \frac{i}{k}\nabla_\perp \cdot \nabla_s - \frac{ik}{2}\left[\mu_D\left(\mathbf{x}_\perp + \frac{\mathbf{s}}{2}\right) - \mu_D\left(\mathbf{x}_\perp - \frac{\mathbf{s}}{2}\right)\right]\right)\{\hat{\Gamma}\} = 0. \quad \text{(A2)}$$

In order to obtain Eq. (6) the additional approximation

$$\mu_D(\mathbf{x}_\perp + \mathbf{s}/2) - \mu_D(\mathbf{x} - \mathbf{s}/2) \approx \mathbf{s} \cdot \nabla_\perp \mu_D \quad \text{(A3)}$$

must be made.

The validity of this approximation, which may be termed a locally quadratic approximation, is discussed in Ref. 1. We do not yet have enough experience to know how often the conditions for the validity of Eq. (A3) are met in practice. It should thus always be kept in mind that, if necessary, we can consider numerically solving for $\{\hat{\Gamma}\}$ using the full difference term given in (A2). In the absence of scattering, this is clearly feasible when μ_D depends only on the depth direction.

If we do not make the approximation given in (A3) and wish to consider $\{\tilde{\Gamma}(\mathbf{x}, \theta)\}$ rather than $\{\hat{\Gamma}(\mathbf{x}, \mathbf{s})\}$ the term $\frac{1}{2}(\nabla_\perp \mu_D) \cdot \nabla_\theta$ is replaced by the convolution of $\{\Gamma\}$ and

the Fourier transform of the difference $\mu_D(\mathbf{x}+\mathbf{s}/2) - -\mu_D(\mathbf{x}-\mathbf{s}/2)$ with respect to $\mathbf{s}$. The final term is

$$\frac{\bar{k}^3}{2\pi}\int \mathrm{Im}\left(\tilde{\mu}_D[2\bar{k}(\boldsymbol{\theta}-\boldsymbol{\theta}')]\exp[2i\bar{k}(\boldsymbol{\theta}-\boldsymbol{\theta}')\cdot\mathbf{x}_\perp]\right) \times\{\tilde{\Gamma}(\mathbf{x},\boldsymbol{\theta}')\}\,d\boldsymbol{\theta}', \tag{A4}$$

where $\tilde{\mu}_D$ is the Fourier transform of μ_D.

APPENDIX B: VALIDITY OF THE SCATTERING TERMS IN EQ. (1)

The scattering terms in Eq. (1) are valid provided that in the distance l_H significant diffraction or refraction does not occur. If l_H is of the order of 10 or more kilometers, this condition is sometimes not satisfied (particularly with respect to refraction effects) and Eq. (1) is not valid.

As of the writing of this article, the authors are not aware of any modifications of Eq. (1) that account for significant refraction within a distance l_H. It is, however, possible in principle to include such an effect by using the method the authors used to derive the integro-differential equation governing $\{\hat{\Gamma}\}$ in the highly anisotropic case. Here, we should have to solve a difference, rather than differential, equation in z, for the scattering integral Green's functions would include refraction effects. Whether or not the result would be useful would depend upon how much the scattering integral could be simplified.

APPENDIX C: DERIVATION OF THE QUASI-ISOTROPIC AND HIGHLY ANISOTROPIC APPROXIMATIONS FROM THE SCATTERING TERM IN EQ. (2)

From the expression

$$\tilde{\sigma}_G(\boldsymbol{\theta},\boldsymbol{\theta}') = \int \sigma(\mathbf{u})\exp[i\bar{k}(\boldsymbol{\theta}-\boldsymbol{\theta}')\cdot\mathbf{u}]\,d\mathbf{u}, \tag{2}$$

the quasi-isotropic and highly anisotropic approximations may be easily found. Since our entire theory is restricted to small angle scattering about the mean propagation distance z, we have

$$\{|\theta_x|, |\theta_x'|, |\theta_y|, |\theta_y'|\} \ll 1.$$

Therefore,

$$\theta_z = (1-\theta_x^2-\theta_y^2)^{1/2} \approx 1 - \theta_x^2/2 - \theta_y^2/2,$$

and Eq. (2) becomes

$$\tilde{\sigma}_G(\boldsymbol{\theta},\boldsymbol{\theta}') = \int\int\int \sigma(\mathbf{u})\exp\left(i\bar{k}[(\theta_x-\theta_x')u_x + (\theta_y-\theta_y')u_y - \tfrac{1}{2}(\theta_x^2-\theta_x'^2)u_z - \tfrac{1}{2}(\theta_y^2-\theta_y'^2)u_z]\right) du_x\,du_y\,du_z. \tag{C1}$$

Here, terms of order $\frac{1}{8}(\bar{k}\theta_x^4 u_z)$ and $\frac{1}{8}(\bar{k}\theta_y^4 u_z)$ are assumed to be much less than unity. This condition is met for both limiting cases provided refractive effects are negligible, since

$$\theta_s = O(1/\bar{k}l_H) \quad \text{(isotropic scattering)},$$
$$\theta_s = O(1/(\bar{k}l_H)^{1/2}) \quad \text{(highly anisotropic scattering)}. \tag{C2}$$

Here u_z is of order l_H.

If the refraction angle is large, then these terms may only be neglected if $\bar{k}$ is sufficiently small. Of course we note that if it is possible to follow ray paths (see Sec. II), the effect of a large refraction angle may perhaps be overcome.

To obtain the quasi-isotropic model and the isotropic theory commonly used in the optics literature, we assume

$$\tfrac{1}{2}(\bar{k}\theta_x^2 u_z) \ll 1, \quad \tfrac{1}{2}(\bar{k}\theta_y^2 u_z) \ll 1. \tag{C3}$$

This is only possible if

$$\theta_y \ll (\tfrac{1}{2}\bar{k}l_H)^{-1/2}. \tag{C4}$$

(We note that θ_{sx} satisfies the necessary condition.)

To obtain the highly anisotropic model we require

$$\tfrac{1}{2}(\bar{k}\theta_x^2 u_z) \ll 1, \quad \bar{k}\theta_y u_y \ll 1. \tag{C5}$$

The condition on θ_x is satisfied, but the second condition leads to

$$\theta_y \bar{k} l_V \ll 1. \tag{C6}$$

Ignoring refraction for the moment, we see that the parameter that determines which limit is appropriate is

$$\alpha \equiv (\bar{k}l_V^2/l_H).$$

If $\alpha \gg 1$, then a quasi-isotropic model is appropriate, and if $\alpha \ll 1$, then a highly anisotropic model is appropriate. If, for example, $l_V = 100$ m and $l_H = 7000$ m, then $\alpha = 1$ when $\bar{k} = 0.7$ m^{-1} (167 Hz). The condition required for the anisotropic model was correctly given in Refs. 10–13. It was incorrectly stated in the survey, Ref. 15.

If refraction angles are significant, Eqs. (C4) and (C6) may be very difficult to satisfy unless it is possible to follow ray paths.

[1] J. J. McCoy and M. J. Beran, "Propagation of Beamed Signals Through Inhomogeneous Media: A Diffraction Theory," J. Acoust. Soc. Am. Suppl. 1 **57**, S64 (1975); J. Acoust. Soc. Am. **59**, 1142–1149 (1976).

[2] A. M. Whitman and M. J. Beran, "Numerical Calculation of the Intensity Distribution in Sound Channels Using Coherence Theory," J. Acoust. Soc. Am. Suppl. 1 **62**, S20 (1977); J. Acoust. Soc. Am. **63**, 1727–1732 (1978).

[3] J. J. McCoy, "Interpretation of Radiation Fields in Terms of Sub-Beams," J. Acoust. Soc. Am. **61**, 923–927 (1977).

[4] J. J. McCoy, "On an Extended Parabolic-Coherence Function Propagation Model," J. Acoust. Soc. Am. **64**, 1703–1709 (1978).

[5] I. M. Besieris and F. D. Tappert, "Kinetic Equations for the Quantized Motion of a Particle in a Randomly Perturbed Potential Field," J. Math. Phys. **14**, 1829–1836 (1973).

[6] F. Tappert, "Diffractive Ray Tracing of Laser Beams," J. Opt. Soc. Am. **66**, 1368–1373 (1976).

[7] I. M. Besieris and F. D. Tappert, "Stochastic Wave-Kinetic Theory in the Liouville Approximation," J. Math. Phys. **17**, 734–743 (1976).

[8] M. J. Beran, "Propagation of a Finite Beam in a Random Medium," J. Opt. Soc. Am. **60**, 518–521 (1970).

[9] V. I. Tatarskii, "Propagation of Light in a Medium with Random Refractive Index Inhomogeneities in the Approximation of the Markov Random Process," Zh. Eksper. Teor. Fiz. **56**, 2106 (1969).

[10] M. J. Beran and J. J. McCoy, "Propagation Through an Anisotropic Random Medium. An Integro-Differential Formula-

tion," J. Math. Phys. **17**, 1186–1189 (1976).
[11]M. J. Beran and J. J. McCoy, "Propagation Through An Anisotropic Random Medium," J. Math. Phys. **15**, 1901–1912 (1974).
[12]M. J. Beran, J. J. McCoy, and B. B. Adams, "Effects of a Fluctuating Temperature Field on the Spatial Coherence of Acoustical Signals," Naval Research Laboratory Report 7809, 22 May 1975, Washington, DC.
[13]V. I. Tatarskii, "The Effects of the Turbulent Atmosphere on Wave Propagation," translated from Russian by Israel Program for Scientific Translations, Jerusalem, TT-68-50464, 472 pp., National Technical Information Service, U. S. Dept. of Commerce, Springfield, VA (1971).
[14]A. M. Obukhov, "Scattering of Sound in Turbulent Flow" (in Russian), Dokl. Akad. Nauk SSSR **30**, 611 (1941).
[15]M. J. Beran, "Coherence Equations Governing Propagation Through Random Media," Radio Sci. **10**, 15–21 (1975).
[16]S. M. Flatte, R. Dashen, W. H. Munk, F. Zachariasen, "Sound Transmission Through a Fluctuating Ocean," Technical Report JSR-76-39, Stanford Research Institute, Menlo Park, CA (1977).
[17]D. R. Del Balzo and W. B. Moseley, "Random Temperature Structure as a Factor in Long Range Propagation," SACLANTCEN Conference Proceedings No. 17, Part 6, 30-1 to 30-10, La Spezia, Italy (1975).
[18]S. M. Flatte, "Sound Transmissions Through a Fluctuating Ocean," J. Acoust. Soc. Am. Suppl. 1 **62**, S28 (1977).
[19]R. D. Dashen, "Path Integrals for Waves in Random Media," J. Acoust. Soc. Am. Suppl. 1 **62**, S29 (1977).
[20]M. Leitman, N. Schwartz, and M. J. Beran, "Scattering in the Depth Direction for an Anisotropic Random Medium," J. Math. Phys. **19**, 2121–2123 (1978).
[21]N. Schwartz, "The Propagation of Acoustic Radiation Through an Anisotropic Medium," Ph.D. thesis, Tel-Aviv University, 1978.

Appendix E

SAMPLE RUN

In this appendix we present the input data and computed results from two runs of COVERT, one run using the general calculation and the other using the high-frequency or quasi-isotropic algorithm. We chose parameters so that α would be 2.0, which is the established value for changing algorithms. Both runs were made on the VAX 11/780 at NRL, Code 5160.

For our example we chose a profile characteristic of the Blake plateau region of the Atlantic (Fig. E1). Using TRIMAIN,* we traced the zero-degree ray from a source depth of 1000 m to a range of 100 km. We saved the depth of the ray every 2.0 km, producing the segmented macroray path shown in Fig. E2. The exact data input to COVERT is shown in Table E1.

The fluctuation-strength profile is also characteristic of the Atlantic and the data input to COVERT is shown in Table E2.

We chose a source frequency of 334.225 Hz and correlation lengths of $l_V = 100.0$ m, and $l_H = 7000.0$ m. Then $\alpha = k_0 l_V^2 / l_H = 2.0$, which is the established value for changing to the high-frequency algorithm. We made two runs, using the the two algorithms.

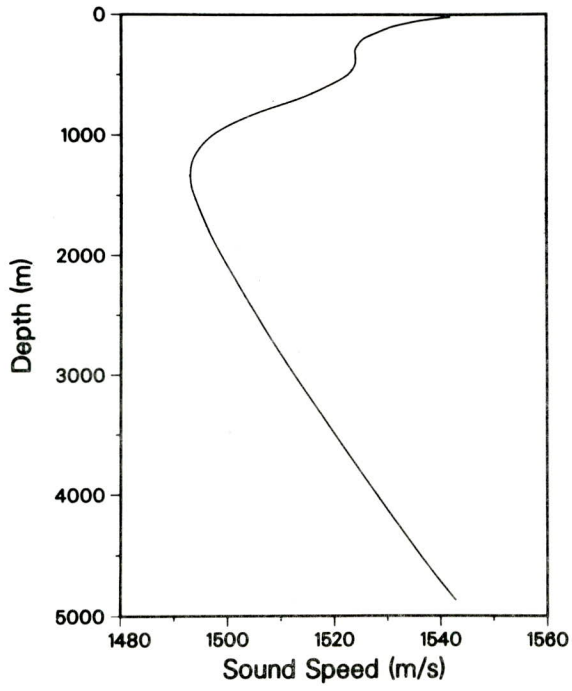

Fig. E1 — Sound-speed profile, characteristic of the Blake plateau region of the Atlantic, used to generate the segmented ray path of Fig. E2

*B.G. Roberts Jr., "Horizontal-Gradient Acoustical Ray-Trace Program TRIMAIN," NRL Report 7827, Dec. 1974.

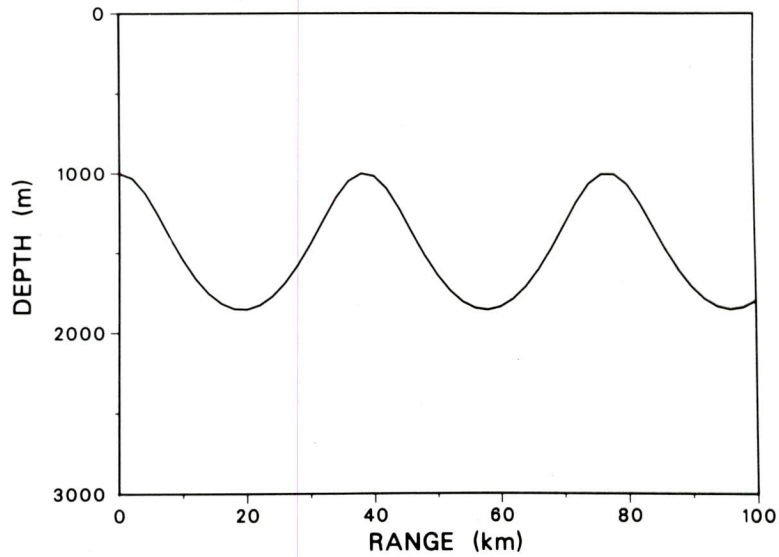

Fig. E2 — Segmented macroray path input to COVERT for the sample runs in Appendix E

Table E1—Ray-Path Input Data Used for the COVERT Sample Runs

Range (km)	Depth (m)	Range (km)	Depth (m)	Range (km)	Depth (m)	Range (km)	Depth (m)
0.0	1000.0	26.0	1688.0	52.0	1735.0	78.0	1009.0
2.0	1032.0	28.0	1578.0	54.0	1806.0	80.0	1072.0
4.0	1125.0	30.0	1444.0	56.0	1846.0	82.0	1191.0
6.0	1260.0	32.0	1296.0	58.0	1857.0	84.0	1337.0
8.0	1409.0	34.0	1154.0	60.0	1838.0	86.0	1483.0
10.0	1548.0	36.0	1049.0	62.0	1789.0	88.0	1611.0
12.0	1664.0	38.0	1002.0	64.0	1711.0	90.0	1714.0
14.0	1755.0	40.0	1018.0	66.0	1607.0	92.0	1791.0
16.0	1818.0	42.0	1097.0	68.0	1478.0	94.0	1839.0
18.0	1852.0	44.0	1225.0	70.0	1332.0	96.0	1857.0
20.0	1855.0	46.0	1373.0	72.0	1186.0	98.0	1845.0
22.0	1829.0	48.0	1516.0	74.0	1069.0	100.0	1804.0
24.0	1773.0	50.0	1638.0	76.0	1008.0		

Table E2—Fluctuation-Strength Input Data Used for the COVERT Sample Runs

Depth (m)	E	Depth (m)	E	Depth (m)	E
0.0	0.218E-10	300.0	0.456E-10	1250.0	0.122E-09
30.0	0.384E-10	400.0	0.407E-10	1500.0	0.534E-10
70.0	0.906E-10	500.0	0.518E-10	1750.0	0.166E-10
100.0	0.123E-09	600.0	0.660E-10	2000.0	0.193E-10
150.0	0.119E-09	700.0	0.789E-10	2500.0	0.721E-11
200.0	0.973E-10	800.0	0.963E-10	3000.0	0.500E-11
250.0	0.605E-10	1000.0	0.138E-09	4000.0	0.500E-11

Some of the results from these two runs are shown for comparison in Table E3. The *Total Signal* plots are shown in Fig. E3, and the *Normalized Scattered Signal* plots are shown in Fig. E4. As can be seen from the table and the plots, there are essentially no differences in the computed results.

In the general formulation run, the calculation required 191 iterations for an average of 3.82 iterations for each of the 50 segments of the macroray path. The high-frequency algorithm is obviously much faster, but the computation time of the low-frequency algorithm is not unreasonable considering its relative complexity.

Table E3—Summary of Results from the COVERT Sample Runs

	General Formulation	High-Frequency Formulation
Total normalized range	6.60	6.72
Final characteristic length	153.2 m	148.5 m
Final characteristic angular width of scattered signal	1.24°	1.31°
Peak of total signal	0.012	0.011
Total CPU time required	745 s	79 s

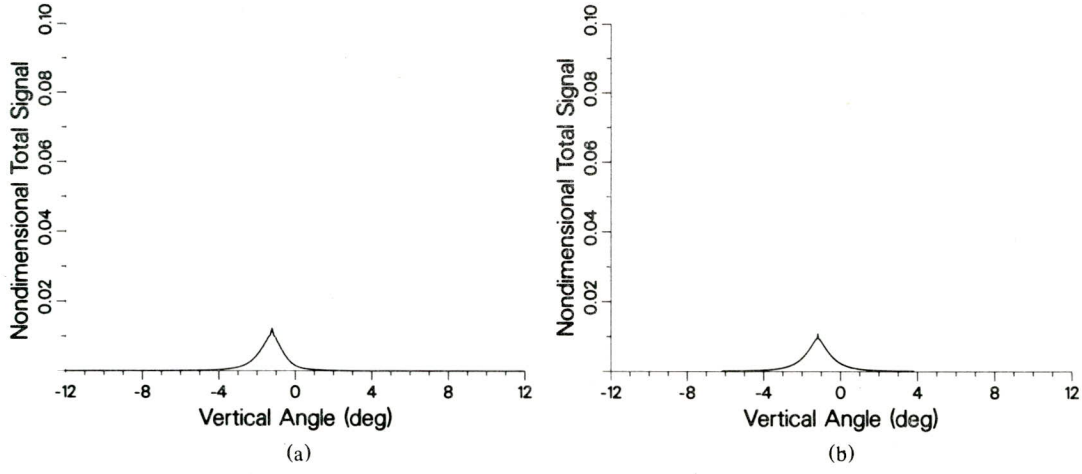

Fig. E3 — Total signal plots from the sample runs. (a) general formulation result; (b) quasi-isotropic result.

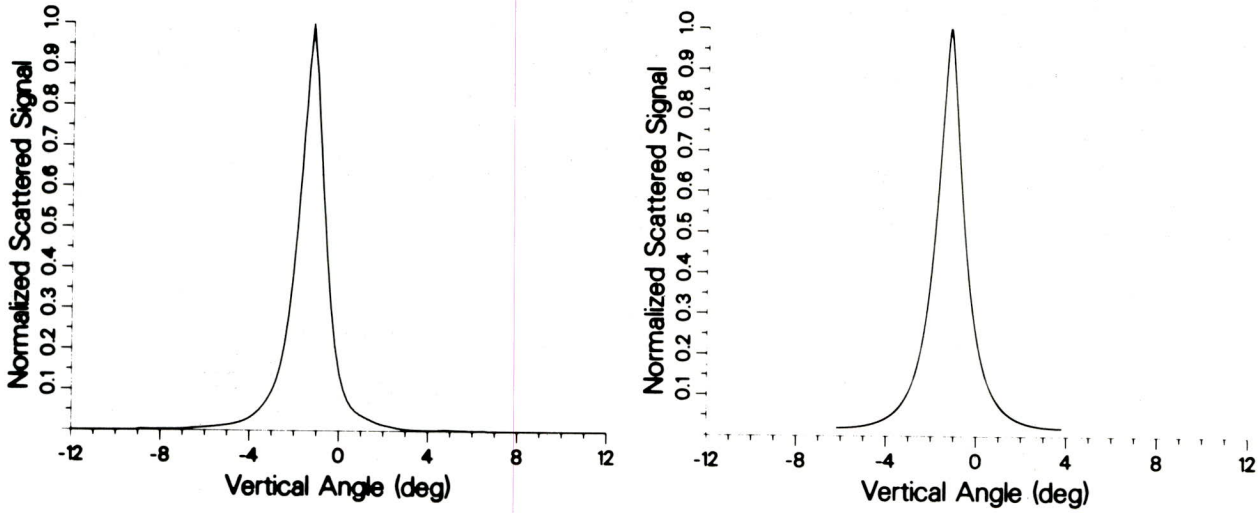

Fig. E4 — Normalized scattered signal plots from the sample runs.
(a) general formulation result; (b) quasi-isotropic result.